



---

Deliverable 3.5  
**DELIVERY OF LIGHTWEIGHT  
BEAM FOR CONSTRUCTION**

---

Dissemination level: Public

Date: 31/03/2025



The project has received funding from the European Union's Horizon 2020 Research and Innovation Programme under Grant Agreement No. 952941.

## Document control sheet

<b>Project</b>	BIOMAC – European Sustainable Biobased Nanomaterials Community
<b>Call identifier</b>	H2020-NMBP-TO-IND-2020-twostage
<b>Grant Agreement N°</b>	952941
<b>Coordinator</b>	Aristotelio Panepistimio Thessalonikis - AUTH
<b>Work package N°</b>	3
<b>Work package title</b>	Pilot Plant Supreme Hub (PPSH)
<b>Work package leader</b>	LIST
<b>Document title</b>	Delivery of lightweight beam for construction
<b>Lead Beneficiary</b>	
<b>Dissemination level</b>	Public
<b>Authors</b>	ACCIONA
<b>Contributors</b>	EUBIA,BBEP,UEDIN,LIST, AIMEN,ACCIONA
<b>Reviewer(s)</b>	LIST, AUTH
<b>Issue date</b>	

### DOCUMENT HISTORY

Date	Version (n.)	Summary of changes
14/03/2025	1	Draft
17/03/2025	2	Included UEDIN & ACCIONA contributions
31/03/2025	3	Final spelling and grammar checking

## Table of Contents

1	Abbreviations .....	4
2	Executive Summary .....	4
3	TeC 4 – Construction.....	4
3.1	PL 5 – Hydrothermal pre-treatment of biomass - BBEPP .....	5
3.2	PL 10 – Mechanical milling and Production of different grades of nanofibrillated cellulose NFCs - LIST .....	5
3.3	PL 8 – Biomass carbonization - UEDIN .....	6
3.4	PL 9 – Melt Compounding - LIST.....	6
3.5	PL15 – Additive manufacturing - AIMEN.....	6
3.6	Tec 4 -ACCIONA .....	7
4	Progress and Achievements .....	7
4.1	PL 5 – Hydrothermal pre-treatment of biomass - BBEPP .....	7
4.2	PL 10 – Mechanical milling and Production of different grades of nanofibrillated cellulose NFCs - LIST .....	10
4.2.1	Processing System and Modifications .....	10
4.2.2	Grinding Process.....	11
4.2.3	Characterization of NFC.....	11
4.2.4	Particle Size and Morphology.....	11
4.2.5	Energy Consumption and Optimization.....	13
4.2.6	Structural and Rheological Properties .....	14
4.2.7	Application in Nanocomposites .....	14
4.3	PL 8 – Biomass carbonization - UEDIN .....	15
4.4	PL 9 – Melt Compounding - LIST .....	17
4.4.1	Selection of raw materials and range of compositions based on PLA:.....	18
4.4.2	PL9 / melt-compounding of nano-composite based on PLA:.....	19
4.5	PL15 -AIMEN.....	22
4.5.1	Printability tests on commercial PLAs .....	22
4.5.2	Printability tests on BIOMAC based PLA bio-compounding.....	25
4.5.3	4. Demo manufacturing.....	28
4.6	Tec 4 ACCIONA .....	36
5	Conclusions.....	44

# 1 Abbreviations

AIMEN	Asociación de Investigación Metalúrgica del Noroeste
AM	Additive Manufacturing
BBEPP	Bio Base Europe Pilot Plant
EUBIA	European Biomass Industry Association
LIST	Luxembourg Institute of Science and Technology
GF	Glass fibre
PL	Pilot Line
UEDIN	University of Edinburgh
TeC	Test Case
NIPUs	Non-Isocyanate Polyurethanes
PLA	Poly(lactic acid)
MISC	Miscanthus

# 2 Executive Summary

This deliverable outlines the various steps undertaken in the fabrication and construction of the demonstrator for [TEST CASE 4](#). The demonstrator consists of a 1:7 scale footbridge built using a thermoplastic biopolymer developed within the BIOMAC project and manufactured through 3D printing technology.

Throughout this work, the developments carried out by each pilot plant to produce the demonstrator’s different materials are reviewed, including the main biopolymer, poly(lactic acid) (PLA), as well as the additives (NFC, lignin, Biochar). Additionally, the design and construction process of the demonstrator is detailed. To determine the design parameters, various mechanical tests and material simulations were conducted, defining both the material properties and the structural requirements of the final construction.

The final footbridge design is modular, featuring a structural base made of a 3D-printed biopolymer lattice reinforced with fiberglass panels. Various additional panels and railings are attached to this base, showcasing the versatility of 3D printing in modifying the aesthetics of such structures.

# 3 TeC 4 – Construction

The objective of TeC 4 was the construction a footbridge by FGF based on a biobased polymer. With this view the biobased (nano)fillers (i.e., cellulose, lignin and biochar) of the (nano-composite) NC were developed based on feedstock from the consortium. The specifications of this material were defined by ACCIONA and AIMEN by analyzing the physical and mechanical requirements covering the printability by FGF and the applicability in the construction sector. Then, LIST worked on the compounding while BBEPP, and UEDIN were responsible for providing the necessary fillers.

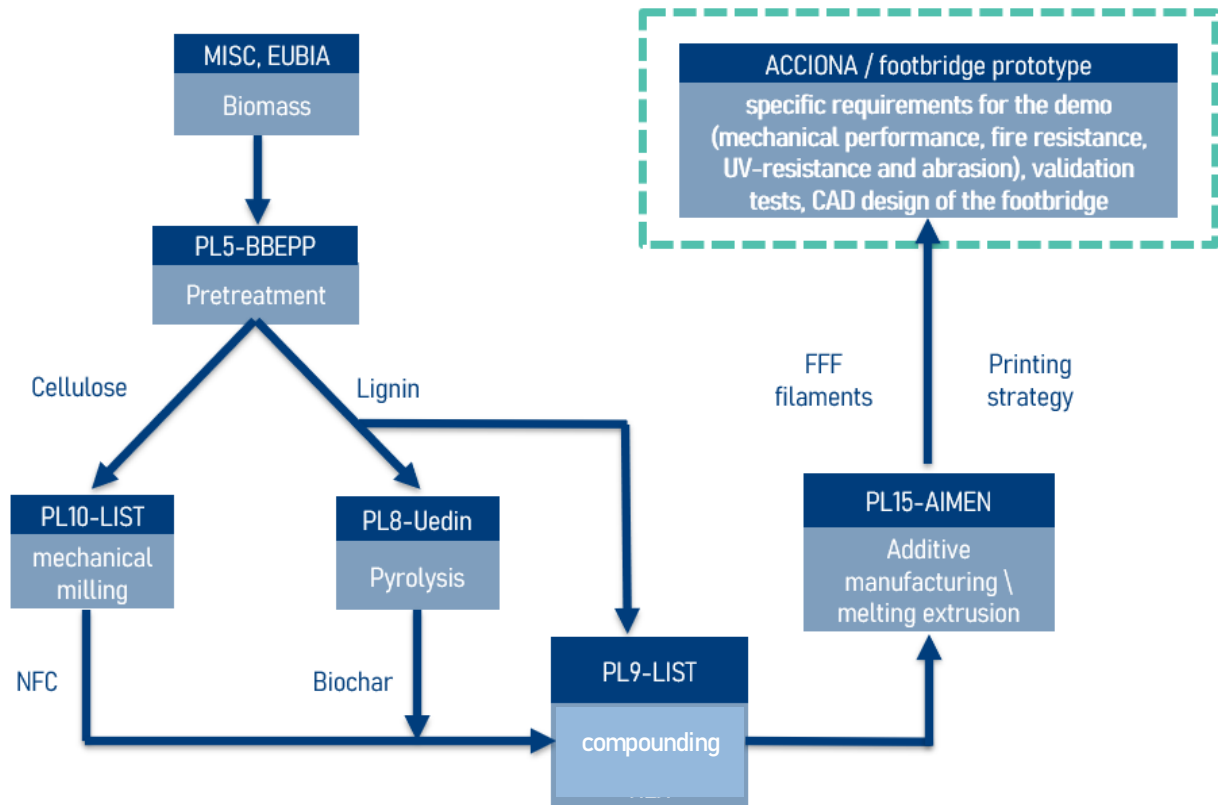


Figure 1: Tec 4 Process Flow and Pilot involved

The following provides a more detailed overview of the Pilot Plants Involved in the development of this demonstrator.

### 3.1 PL 5 – Hydrothermal pre-treatment of biomass - BBEPP

The role of BBEPP was to pretreat the biomass (miscanthus) and separate the 3 lignocellulosic fractions from each other on lab and pilot scale. The first approach was to establish a suitable lab protocol, followed by a pilot run in order to gain enough application material, such as lignin and cellulose to send to partners [Uedin \(PL8\)](#) and [LIST \(PL9,10\)](#).

### 3.2 PL 10 – Mechanical milling and Production of different grades of nanofibrillated cellulose NFCs - LIST

One of LIST's role was the production of nanofibrillated cellulose (NFCs). Nanocellulose substrates in the form of NFCs were produced through mechanical shearing of pure cellulosic fibers or cellulose fibers with varying compositions, particularly different residual lignin content. All cellulose sources will be obtained from the [PL1- Semi-continuous organosolv-steam explosion pre-treatment](#)-LTU facility.

This technology enables the processing of both short and long cellulose fibers with diverse compositions while maintaining low energy consumption and avoiding clogging issues commonly found in other

technologies. The treatment parameters can be adjusted to produce NFCs with the desired aspect ratio (Length/Diameter). When necessary, oxidative chemical pre-treatments will be applied to soften the fibers before mechanical processing. Additionally, post-chemical modifications can be performed on the resulting NFCs to enhance compatibility with polymeric matrices or introduce specific functional properties. The final NFCs will be incorporated into polymeric (nano)materials tailored for targeted applications.

### 3.3 PL 8 – Biomass carbonization – UEDIN

[UEDIN's pilot plant](#) purpose is to produce biochar. The pyrolysis process that UEDIN performs in its plant obtains highly porous solid carbons, phenol-rich liquids, and combustible gases. The solid carbons feature tunable surface functionality and controllable electrical conductivity, making them suitable for use in packaging polymer additives, printed electronics, building materials, animal feed additives, and agricultural applications such as fertilizers and soil amendments.

This plant is capable of reliably, efficiently, and safely processing biomass into high-value products, such as porous solid carbons and phenol-rich liquids, up to TRL7.

### 3.4 PL 9 – Melt Compounding – LIST

The second role of LIST in the Tests Case is the compounding of the additives with the thermoplastic. The reactive extrusion of thermoplastic polymers has been conducted using an 18 mm [twin-screw extruder](#) equipped with six gravimetric solid feeders, enabling continuous processing. This approach offers significant advantages over traditional batch polymerization processes, which are less flexible in terms of processing conditions.

### 3.5 PL15 – Additive manufacturing – AIMEN

The [pilot plant of AIMEN](#) consists of a 3D printing robotic arm and it is the technology used for the footbridge production. This PL consists in a filament/pellet production station and large format printing cell includes a Robot Printing Arm and a extruder (CEAD'S pellet based robot extruder) altogether with CEAD's large heated printed (3x1.2m) table that enables large format robotized additive manufacturing technology, allowing to process virtually any thermoplastic polymer suitable for 3D printing. Pictures a and b of Figure 2 show pictures of the current PL15 cell and a detail of the pellet's extruder purchased from CEAD. To complete PL15 upgrading a Filament Extruder Station and a pelletizer (showed in c and of Figure 2) purchased from Machine AB KFM Sweden were as well incorporated. Pelletised material obtained from the extruder station can already be directly 3D printed using the LFAM cell robot extruder avoiding the filament winding step.



Figure 2: PL15 upgrading a) robotized cell, b) pellets extruder, c) extrusion station and d) pelletizer.

### 3.6 Tec 4 -ACCIONA

Acciona evaluated the material and provided technical and construction specifications to adapt the developed project material to the construction sector. They also created numerical models and design a digital footbridge based on the results of initial mechanical specimen tests. Finally, Acciona received the different printed modules produced using PL15 technology and assembled them to create the final demonstrator.

## 4 Progress and Achievements

### 4.1 PL 5 – Hydrothermal pre-treatment of biomass - BBEPP

The BIOMAC pilot run has produced sufficient materials for the partners to use in further testing applications. The sequential acid/base pretreatment helps to achieve a purer lignin and glucose stream because of the prior separation of a large part of the hemicellulose. As is always the case, complete separation of the lignocellulosic biomass was not possible. Despite the difficult separation, the pilot run has yielded relatively pure streams – some of which could be purified further if necessary (f.e. bleaching of cellulose solids).

In the following the objectives are shortly explained:

- I. Biomass pretreatment Miscanthus – Step-by-step approach  
Received biomass (500kg) miscanthus (*Miscanthus giganteus* clone) from partner Miscanthus.
  - i. Evaluation on the different fractions to decide to continue with the smallest fraction (smallest fraction < 5 mm) for further size reduction.

- ii. Physical size reduction of biomass with Stephan miller cutter to determine best size for pilot run
- b. Lab and pilot biomass pretreatment runs: Sequential pre-treatment of biomass under acidic and alkalic conditions. Pretreatment under only alkalic condition is also performed separately to compare with sequential pretreatments.
- c. Production of end products to be used by partners: Cellulose-rich solids, hemicellulose filtrate, lignin.
- d. Production of lignin to be analyzed off-site
- e. Milling with Stephan miller of end-product lignin from pellets to reduce size into powder state

The most important steps of the biomass pretreatment process are summarized in Figure 3, together with a short description of each process step.

Step	Description
1	Pulping The Miscanthus biomass is mixed into a slurry using the big pulper.
2	Acid pretreatment The slurry from step 1 gets an acidic pretreatment using 1% H <sub>2</sub> SO <sub>4</sub> at 85°C for 6 hours. This will separate the hemicellulose from the biomass and split it into monosaccharides.
3	Filtration after acid pretreatment The pre-treated slurry is filtered using a chamber filter press fitted with the new cloths that were bought after the lab tests in F01. The filtrate contains the hemicellulose while the solids are further pre-treated. The filtrate is concentrated in step 4 while the leftover solids will undergo an alkalic pre-treatment.
4	Wiped film evaporation of hemicellulose The acidic hemicellulose filtrate is neutralized before being concentrated using a wiped film evaporator.
5	Alkalic pretreatment The solids obtained from filtration in step 3 are re-solubilized into a slurry. Sodium hydroxide solution is then added until a concentration of 2 v/v% is obtained. The slurry is heated to 85°C for 12 hours after which it is cooled down. The alkalic pre-treatment solubilizes the lignin contained in the biomass.
6	Filtration after alkalic pretreatment Solid-liquid separation after the alkalic pretreatment using the chamber filter press. The filtrate is rich in lignin while the leftover solids contain mostly cellulose.
7	Lignin precipitation The lignin filtrate from step 6 is acidified to precipitate the lignin. The lignin solids can then be separated using the chamber filter press.
8	Drying of end products The cellulose solids and lignin that were harvested during steps 6 and 7 respectively, are dried in the vacuum tray dryer to get dry end products.

Figure 3: Summary of the biomass pretreatment protocol

Cellulose-rich solids		
	Amount	➤ 80 kg
	Packaging	Buckets
	Storage conditions/location	Warehouse, room temperature



Figure 4: Cellulose final product description

Lignin		
	Amount	40 kg
	Packaging	Buckets
	Storage conditions/location	Warehouse, room temperature

Figure 5: Lignin final product description

Material delivery overview of the different fractions to the project partners.

- f. July 2022 Lab delivery of end-product to
  - i. LIST (1kg Lignin)
  - ii. UEDIN (10kg lignin)
- g. January 2023 Lab delivery of end-product to
  - i. LIST (20kg lignin)
  - ii. UEDIN (100kg Lignin)
- h. June 2023 Pilot delivery of end-product to
  - i. LIST (20kg Cellulose)
- i. July 2024 Pilot delivery of end-product milled to
  - i. LIST (40kg powder lignin)

## 4.2 PL 10 – Mechanical milling and Production of different grades of nanofibrillated cellulose NFCs - LIST

### 4.2.1 Processing System and Modifications

Nanofibrillated cellulose (NFC) was produced using an ultra-fine friction grinding approach coupled with a continuous circulation system. The process utilized a Masuko Supermasscolloider equipped with silicon carbide (SiC) grinding stones, which facilitated controlled mechanical fibrillation of cellulosic feedstock. The production system was modified to enable continuous operation, incorporating a pump-controlled recirculation loop, an in-line viscometer for real-time viscosity monitoring, and power consumption meters to assess energy efficiency (see Figure 6).

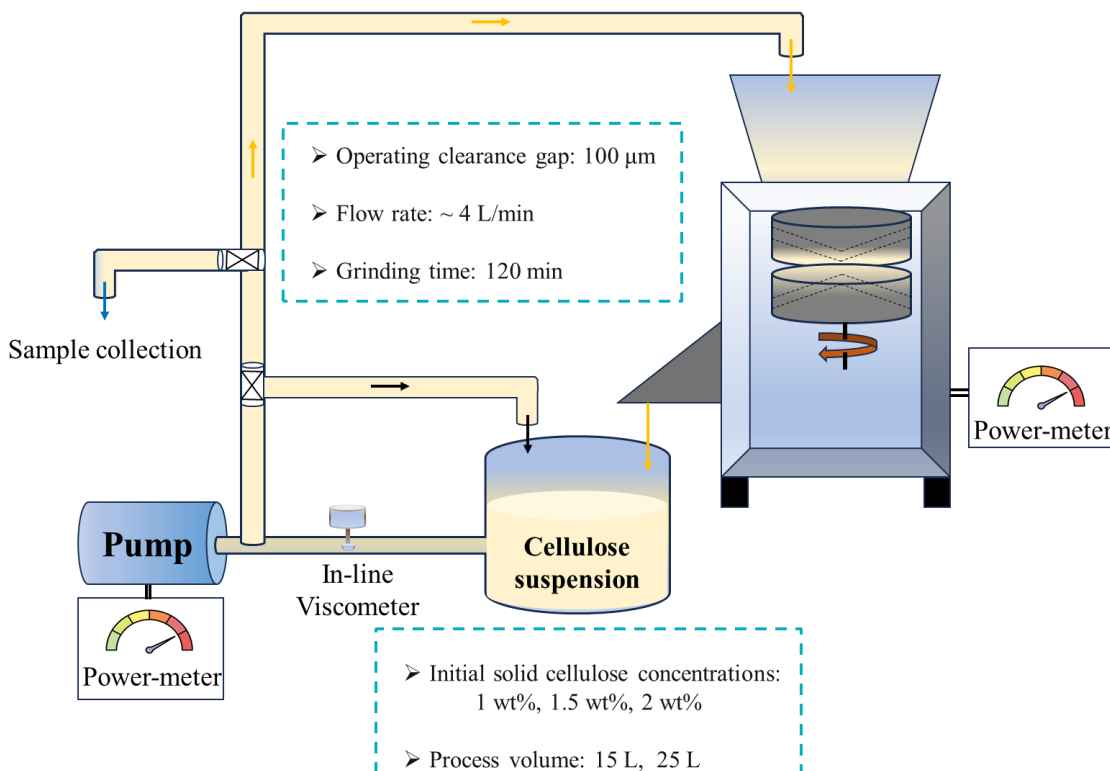


*Figure 6. Schematic diagram of continuous production of nanofibrillated cellulose (NFC) using an ultra-fine friction grinding machine with recirculation system. The black arrows indicate the soaking cycle, the yellow arrows indicates the flow path of the materia*

The biomass used in this study was provided by the [Bio Base Europe Pilot Plant \(BBEPP\)](#).

The raw material used for NFC production was lignocellulosic biomass derived from *Miscanthus*, which underwent a sequential acid-alkaline pretreatment to enhance fiber accessibility. The dried feedstock was initially dispersed in water to achieve a homogeneous cellulose suspension with varying solid contents (1, 1.5, and 2 wt%). This suspension was transferred into a collection tank and pre-soaked for 10 minutes before being introduced into the grinding system.

#### 4.2.2 Grinding Process

Grinding was performed in two sequential stages; first stage: The grinding gap was set to 400  $\mu\text{m}$  for an initial breakdown of cellulose fibres over a period of five minutes. This coarse grinding step was essential for reducing the bulk fibre size and increasing fibre hydration, thereby facilitating the subsequent fibrillation stage. Second stage: The gap was reduced to 100  $\mu\text{m}$  to achieve further fibrillation. The cellulose suspension was continuously circulated through the system at a controlled flow rate of approximately 4 L/min to ensure consistent processing and prevent material clogging.

#### 4.2.3 Characterization of NFC

Samples were extracted at predefined time intervals (15, 60, and 120 minutes) for characterization. Initial observations of the NFC suspension indicated a progressive transition from a coarse fibre slurry to a homogenous gel-like material as grinding time increased. The particle size distribution results showed that the most significant reduction in fibre size occurred within the first 15 minutes, with large fibre fragments breaking down into smaller nanofibrils. As grinding time increased to 60 minutes, further refinement of the fibrils was observed, with a decrease in the fraction of larger particles and a shift toward a more uniform distribution. By 120 minutes, the particle size distribution reached a steady state, indicating minimal additional fibrillation beyond this point.

#### 4.2.4 Particle Size and Morphology

Particle size analysis was conducted to assess the evolution of fibrillation during the grinding process. The LUMiSizer<sup>®</sup> analytical centrifuge was employed to determine the hydrodynamic diameter of NFC particles, providing insights into particle distribution trends across different processing conditions. The results indicated that NFC particles consistently exhibited hydrodynamic diameters within the 200–300 nm range, regardless of grinding time or initial cellulose concentration. However, extended grinding times resulted in reduced skewness of the size distribution, suggesting an improvement in uniformity and a shift toward a more homogeneous suspension.

To further investigate the morphological development of NFC, scanning electron microscopy (SEM) and atomic force microscopy (AFM) were utilized (see Figure 7).

**SEM Analysis:** The images captured at different stages of grinding demonstrated the progressive disintegration of macroscopic fibre bundles into nanoscale fibrils. The transition from coarser fibres to finely dispersed fibrils was evident, particularly beyond the 60-minute grinding threshold, where a reduction in fibre entanglement was observed.

AFM Analysis: High-resolution AFM imaging provided quantitative insights into fibril dimensions. The nanofibrils obtained had diameters in the range of 20–40 nm, with fibril lengths extending several micrometres, yielding aspect ratios between 250 and 300. The presence of well-dispersed, individualized fibrils reinforced the effectiveness of the grinding process in producing high-aspect-ratio NFC, a critical parameter for nanocomposite applications.

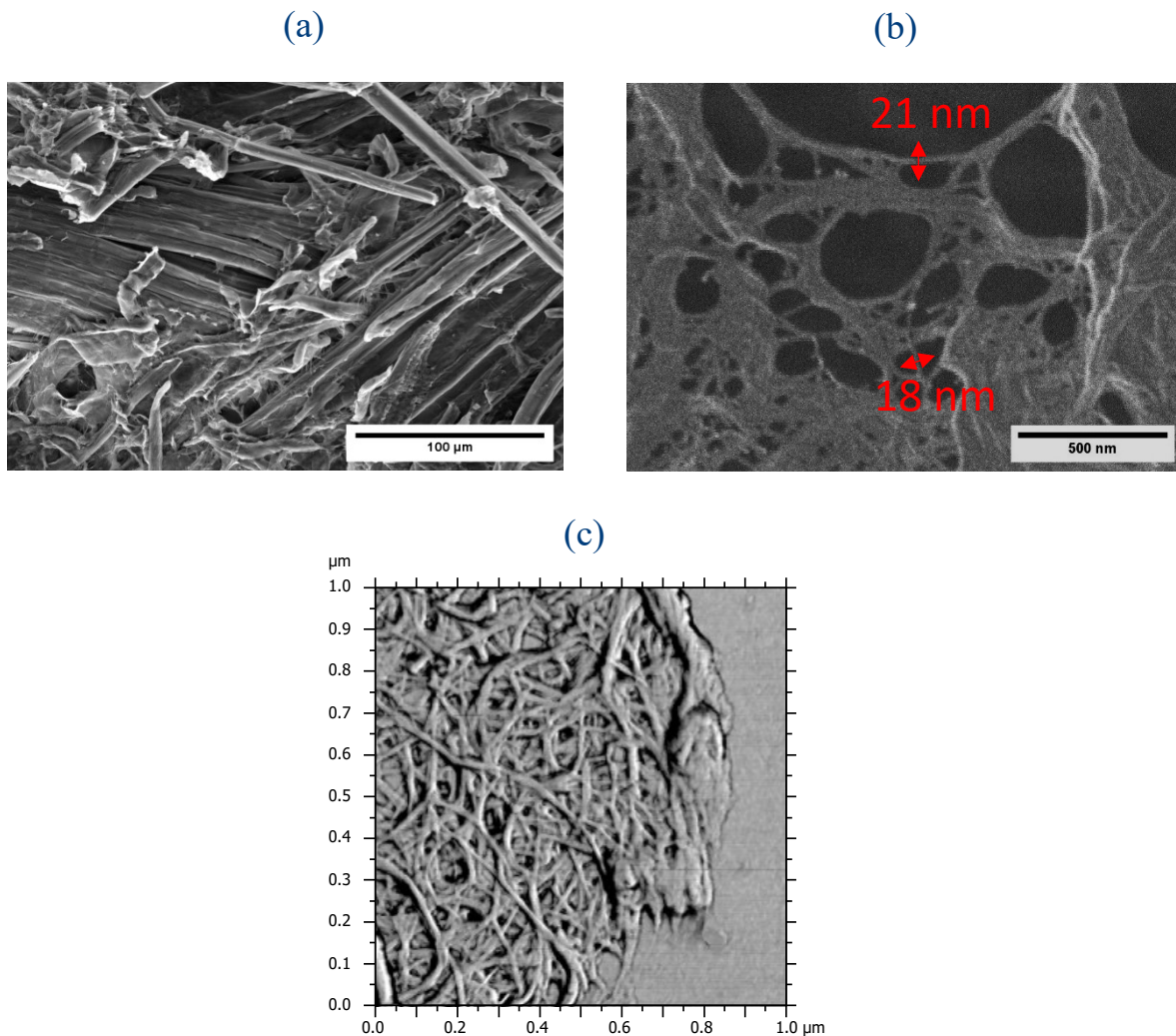


*Figure 7: Scanning Electron Microscope (SEM) images of (a) BBEPP raw lignocellulosic material (scale bar = 100 μm) and (b) freeze-dried NFC (scale bar = 500 nm). (c) A 1 × 1 μm<sup>2</sup> Atomic Force Microscope (AFM) image showing topography of NFC suspension (in ethanol) dried in air onto a glass slide. The NFC suspension was produced following 120 min of continuous processing, using a 2 wt% initial cellulose content and a 25 L process volume.*

Analysis using a LUMiSizer<sup>®</sup> analytical centrifuge confirmed that the equivalent hydrodynamic diameter of the NFC particles remained within the range of 200–300 nm across all processing conditions. However, the skewness of the particle size distribution decreased with longer grinding durations, signifying improved uniformity (Figure 8).

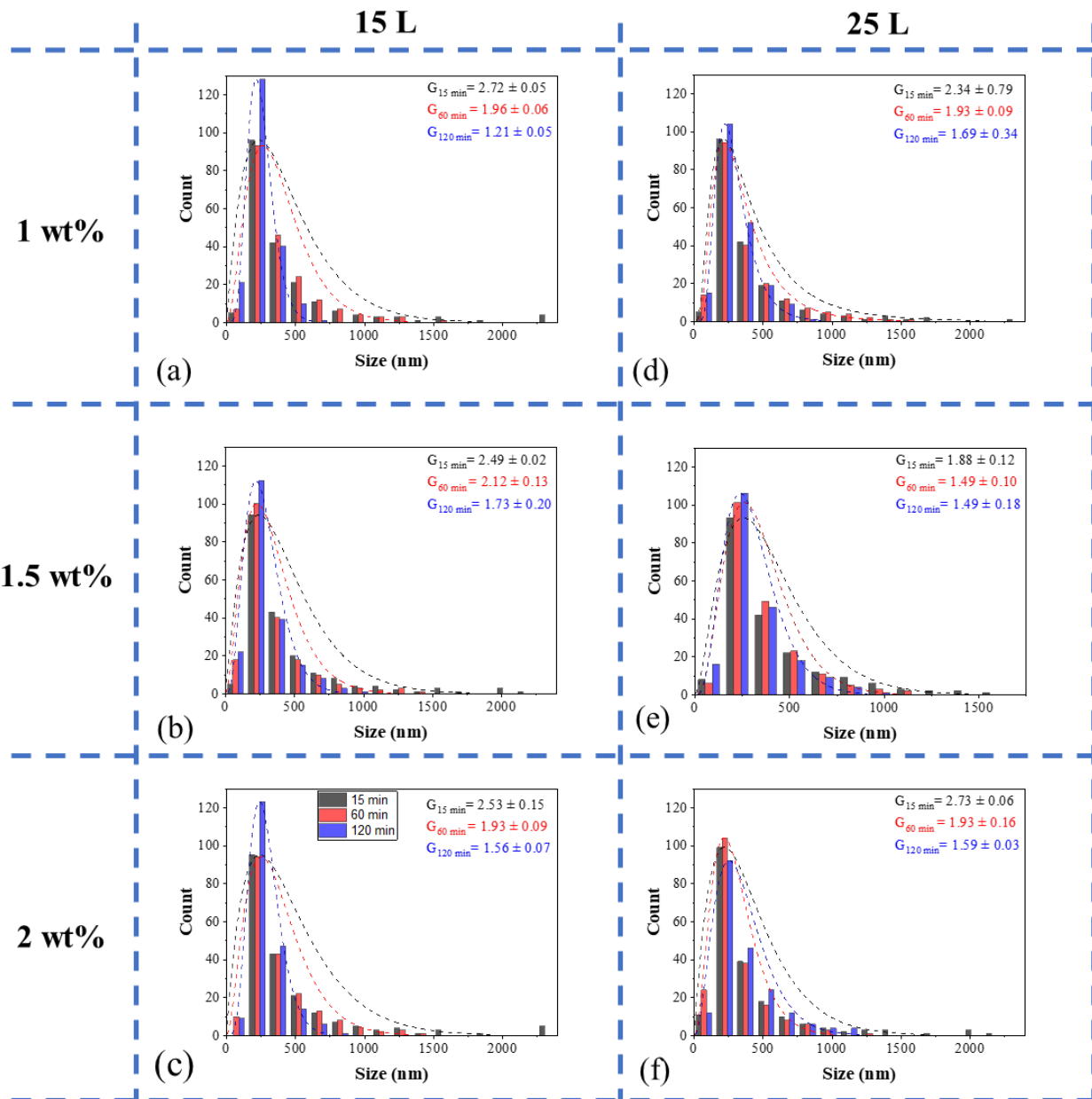


Figure 8: Comparison of particle size distribution histograms with overlaying lognormal distribution curves. Each subplot (a)–(f) represents a different experimental condition, including varying initial cellulose concentrations (1 wt%, 1.5 wt%, and 2 wt%) and process volumes (15 L and 25 L). For each experimental condition, size distribution data were collected at different grinding times (15, 60, and 120 min). The x-axis in each subplot represents equivalent hydrodynamic particle size in nm, while the y-axis indicates the particle count. Bars indicate the observed frequency distribution of particle sizes, while dashed curves represent fitted lognormal distribution curves. Skewness values ( $G$ ) at different grinding times (15, 60, and 120 min) were calculated for each set of processing conditions.

#### 4.2.5 Energy Consumption and Optimization

Specific energy consumption was evaluated by separately measuring the power input for the pumping system and the grinding unit. The data demonstrated a significant reduction in energy consumption when increasing the initial cellulose concentration from 1 wt% to 2 wt% and scaling the process volume from

15 L to 25 L. These optimizations resulted in a 70% reduction in specific energy consumption, reducing the energy input from 32.4 kWh/kg to 9.7 kWh/kg.

#### 4.2.6 Structural and Rheological Properties

The structural properties of the NFC were assessed using X-ray diffraction (XRD) to determine the impact of mechanical grinding on cellulose crystallinity. The diffraction patterns of NFC samples processed under different conditions revealed no significant change in the characteristic cellulose I crystalline peaks, confirming that the fundamental crystalline structure was preserved. This suggests that the applied mechanical forces were sufficient to induce fibrillation without causing excessive disruption to the crystalline domains of cellulose.

Additionally, the crystallinity index (CrI) of the NFC samples was calculated, revealing only minor variations across different grinding times and process conditions. The results indicated that longer grinding durations did not lead to substantial degradation of the crystalline regions, suggesting that energy input could be optimized without compromising structural integrity.

Rheological measurements provided further insights into the dispersion quality of NFC suspensions. Shear-thinning behaviour was observed across all samples, indicative of strong interactions between fibrils within the suspension. Higher initial cellulose concentrations resulted in increased viscosity, reflecting the formation of a denser fibrillar network. The frequency sweep tests confirmed the gel-like nature of the NFC suspensions, with the storage modulus ( $G'$ ) consistently exceeding the loss modulus ( $G''$ ), reinforcing the formation of a well-entangled nanofibril network.

The structural integrity of the NFC was assessed using X-ray diffraction (XRD), revealing that the crystalline fraction of cellulose remained preserved throughout the grinding process. Rheological analysis confirmed the shear-thinning behaviour of NFC suspensions, indicative of a well-dispersed fibrillar network.

#### 4.2.7 Application in Nanocomposites

To assess the reinforcing potential and dispersibility of NFC in a polymer matrix, NFC suspensions obtained at different grinding times were incorporated into carboxymethyl cellulose (CMC) nanocomposites. The goal of this work was to inform further processing steps by evaluating how grinding duration influenced NFC performance in nanocomposite applications.

Mechanical testing of the CMC-NFC films demonstrated a significant increase in tensile properties compared to unfilled CMC films. However, no substantial differences in mechanical performance were observed between nanocomposites containing NFC processed for 15, 60, or 120 minutes. This suggests that prolonged grinding does not necessarily enhance reinforcing efficiency beyond a certain threshold, indicating that NFC of sufficient aspect ratio and dispersion quality can be obtained with shorter grinding times (Figure 9).

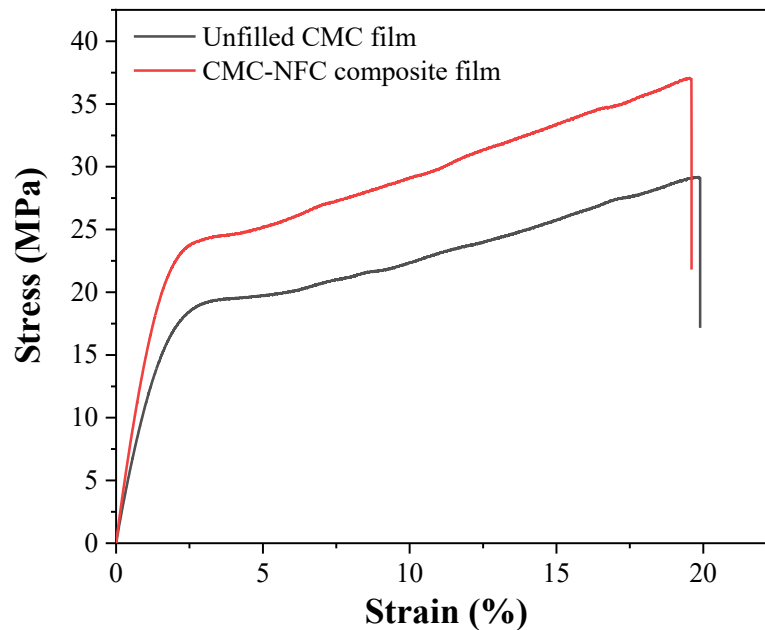


*Figure 9: Representative stress-strain curves of an unfilled CMC film and a CMC-NFC-15min nanocomposite film.*

Additionally, the optical transparency and uniformity of the nanocomposite films suggested effective NFC dispersion within the CMC matrix. AFM surface topography analysis further confirmed the absence of large agglomerates, reinforcing the notion that NFC was well-integrated within the polymer matrix. These findings emphasize the potential for optimizing energy consumption in NFC production while maintaining its effectiveness as a reinforcing agent in biopolymer matrices.

#### 4.3 PL 8 - Biomass carbonization - UEDIN

[PL8](#) was used to produce biochar intended as an additive in PLA compounds. Given uncertainty regarding the precise mixing ratio of biochar in the PLA, the estimated maximum biochar requirement was around 30 kg.

Lignin was originally selected as the preferred feedstock for biochar production, and approximately 100 kg of lignin was delivered to the facility. However, pilot-scale biochar production generally requires a minimum feedstock input of about 50 kg per run to achieve stable operational conditions and consistent product quality. The limited amount of lignin feedstock posed a significant risk: if any production run was unsuccessful or yielded inconsistent biochar quality, there would not have been sufficient feedstock remaining for additional attempts. Consequently, raw Miscanthus biomass, which is the second priority feedstock in the BIOMAC project, was selected as an alternative. Miscanthus was readily available in larger quantities, enabling multiple production attempts, if necessary, thus ensuring greater flexibility and reducing risks associated with potential production challenges.

The biochar production was carried out using the recently upgraded pilot line 8. The pilot line setup includes a twin-screw feedstock hopper designed to provide continuous and uniform feeding of biomass into the reactor. The biomass is conveyed into a rotary kiln reactor, configured as a sealed, rotating cylindrical drum approximately 25 cm in inner diameter and 2.8 meters in length. Heating within the kiln is provided by three independently controlled electric heater banks, each rated at 16.67 kW, enabling precise control of temperature profiles along the reactor. The kiln's operating temperature can be continuously maintained up to a maximum of 850°C, allowing accurate thermal treatment to achieve desired biochar characteristics.

One advantage of the rotary kiln design is its flexibility in controlling feedstock residence times within the reactor. By adjusting the kiln's rotational speed and considering the particle size and shape of the feedstock, residence times can be tailored between 5 to 40 minutes. This capability is critical for optimizing the biochar production process, as the residence time significantly influences the structural integrity, porosity, carbon content, and stability of the produced biochar. After thermal treatment, biochar exits directly into a double-jacketed cooling screw, providing indirect cooling that rapidly lowers the biochar temperature. The cooling stage is essential to prevent oxidation and to maintain consistent physical and chemical characteristics of the biochar.



*Figure 10: Upgraded twin-screw feeding system of pilot line 8 (left). Upgraded gas combustion system (right).*

Prior to scale-up, initial trials were performed using a smaller-scale screw reactor capable of producing approximately 500 g batches of biochar. This smaller system enabled preliminary investigation into the impact of various thermal processing conditions, with particular attention given to temperature effects. Batch trials were systematically conducted across a temperature range from 550°C to 700°C. Pelletized Miscanthus-based biochar produced at 550°C was identified as the most suitable based on preliminary evaluation, showing favourable properties such as appropriate structural integrity, carbon stability, and consistency. This biochar was then sent to LIST for preliminary validation, confirming its suitability for the intended PLA application.

Following successful preliminary tests, detailed production parameters—including peak treatment temperature, residence time within the kiln, rotational speed, and inert gas flow rates—were carefully translated and scaled up to pilot-scale reactor conditions. Specifically, inert gas flow was optimized to

minimize oxygen ingress, thus avoiding unwanted oxidation reactions during production. Using these optimized parameters, pilot-scale production resulted in approximately 50 kg of biochar.

To ensure consistent and uniform material quality, biochar produced during initial reactor stabilization (approximately the first 1.5 hours) and final shutdown stages (approximately the last hour) was discarded. These segments were excluded as they typically present variability in temperature conditions and, consequently, biochar quality. By excluding these variable portions, approximately 30 kg of homogeneous biochar was successfully retained. Half of this biochar (~15 kg) was subsequently packaged and shipped to LIST for further processing, characterization, and integration into the targeted PLA formulations.

These steps established a robust, reproducible pilot-scale production process, ensuring reliable biochar quality and facilitating its integration into subsequent stages of the project. Moreover, this process provided valuable operational insights, particularly concerning feedstock choice, parameter optimization, and reactor performance, contributing beneficially to future scale-up efforts.

*Table 1: Miscanthus Biochar*

<b>Miscanthus biochar</b>	
<i>Highest treatment temperature</i>	550°C
<i>Residence time</i>	25 min
<i>Feeding rate</i>	22 kg hr <sup>-1</sup>
<i>Biochar produced</i>	38.4 kg
<i>Biochar collected</i>	29.8 kg
<i>Biochar yield</i>	21.1 % (w/w)
<i>Carbon content</i>	72.3 % (d.b.)
<i>Fixed carbon content</i>	74.5 % (d.b.)
<i>Bulk density</i>	321 kg m <sup>3</sup>

#### 4.4 PL 9 – Melt Compounding – LIST

Concerning the compounding LIST, with PL9, was responsible for providing a compound based on PLA and biobased (nano)fillers as a raw material for the 3D printing process for the TeC4 prototype. Various trials were performed to improve the properties of the selected biobased composite formulations and optimize their compounding process via twin-screw extrusion. **Given the need to maintain both good mechanical properties and processability, we focused on optimizing the compounding process using PL9 twin-screw extrusion for the compounding of all components.**

#### 4.4.1 Selection of raw materials and range of compositions based on PLA:

Selection of the compositions of the biobased composite was made building upon AIMEN's experience with Fused Filament Fabrication (FFF) and large-scale printing on PL15. We selected as a benchmark a commercial 80/20 w:w PLA / cellulose fibre composite which had interesting printability characteristics (i.e., high speed and no wrapage) and mechanical performances. Notably, when used on PL15 the previously dry formulation exhibited low shrinkage and maintained good processability. Yet, it delivered a rather low Young's Modulus of 11 MPa (cf. Table 2). This significant cellulose fiber load weakened the material without offering an increase in elastic modulus. The inclusion of large amounts of cellulose fibers typically reduces tensile strength, but with appropriate dispersion and interface compatibilization of our biobased fillers (NFC, lignin and biochar), we hypothesized that it could still result in an improved Young's Modulus.

*Table 2: Mechanical testing of printed tensile bars (XY direction). ISO 178*

	Young's modulus (MPa)	Tensile strength (MPa)
PLA (Luminy LX175)	2708	45
PLA / cellulose fibres w:w 80/20	2656	11

We explored the potential of incorporating high percentages of biobased fillers to match the printability of this benchmark composition while ensuring an easy compounding and improved mechanical properties.

Two different polymer matrixes were considered:

- Ingeo Biopolymer 3D850 (NatureWorks): T<sub>g</sub>: 60 °C, melting point: 170 °C, tensile strength (ISO 527): 50 MPa
- Luminy LX175 (TotalEnergies-Corbion): T<sub>g</sub>: 60 °C, melting point: 155 °C, tensile strength (ISO 527): 45 MPa

In an attempt to address these challenges and improve the mechanical performance while preserving processability, various components were selected for their potential synergistic effects:

- NFC (Nanofibrillated Cellulose): Known for its reinforcement potential in polymer matrices.
- Lignin: Anticipated to reduce warping due to its influence on crystallization behavior.
- Biochar: Expected to enhance infrared light absorption and contribute to the thermal stability of the compound.

One of the key questions that arose was the specific mechanical properties we aimed to achieve from these filled compounds. Two approaches can help mitigate warping:

- Crystallization Control: Adding fillers that induce more uniform crystallization.

- Mechanical Reinforcement: Achieved through the effective dispersion and aspect ratio of the fillers.

Drawing from our experience with NFC in polycaprolactone (PCL), high NFC loading was discussed. Specifically, NFC has a high aspect ratio, which leads to a low percolation threshold. Exceeding this threshold can result in poor dispersion, negatively impacting the mechanical properties. Based on previous trials, we found that NFC loading greater than approximately 0.5 – 1 wt% can lead to a decline in performance, especially in terms of mechanical strength.

In terms of lignin and biochar, the consensus was to start with lower filler concentrations (5 wt% each) to avoid overloading the matrix. Higher concentrations (e.g., 10 wt% of each). Therefore, our proposed formulations were aimed at striking a balance between reinforcing the matrix and maintaining optimal dispersion. With this view, the range of targeted formulations was the following: NFC/lignin/biochar w:w:w 0.5 / 5 / 5 - 1 / 10 / 10.

#### 4.4.2 PL9 / melt-compounding of nano-composite based on PLA:

The twin-screw extrusion process allows for the efficient mixing and dispersion of these fillers, which is critical for achieving the desired properties in the final composite material. The primary goal of the following trials was to optimize the throughput and blending quality of the compound in a 18 mm twin-screw extruder while combining the key materials: dried PLA, biochar, lignin, and a masterbatch of nano-cellulose. The trials aimed to overcome the limitations posed by gravimetric feeders and grinders, which had restrictions on feed rates and material characteristics, to achieve an optimal balance between extruder output and homogeneity of the blend. Process conditions were optimized to compound with an output of 10 kg/h for LIST (PL9), a twin-screw extruder (Lesitritz, ZSE Max) having a diameter of 18 mm (L/D 60, which was more than needed for such a compound) and operated under dry nitrogen atmosphere to avoid PLA hydrolysis. The selected formulation was ultimately the following one:

- PLA (Luminy LX175, TOTAL-ENERGIES) : 79,21 wt%
- Grinded biochar (PL8): 9,9 wt%
- Lignin (PL5): 9,9 wt%
- Nano-fibrillated cellulose (PL10): 1 wt%

Key variables in the optimization trials are summarized here below:

- Feedstock pre-processing:

Lignin and biochar were grinded to improve their flowability through the feeders, ensuring consistent input for the extrusion process. A grinder (ZM200, Retsch) using 1 mm ring sieves, at a speed of 10 000 rpm was used. All raw materials were dried to prevent PLA hydrolysis in the melt at 60 °C under reduced pressure of 100 mbar (VO500, Memmert). No addition processing aid was used.

- Feeder rates:

Feeder settings were adjusted to match the raw materials. In particular, lignin powder, after grinding, posed a significant challenge. The powder would often absorb humidity, causing it to clump and block the screws of the gravimetric feeder, requiring the material to be loaded in small batches at frequent intervals to prevent disruptions. Yet the torque of the feeder had to be checked during the production to avoid this equipment to overheat. This issue could be solved by lowering the particle sizes of lignin.

In the case of biochar however, no limitations were observed. None of the fillers produced flow inconsistencies into the extruder or bridging effects. For PLA granules, humidity was controlled by putting the gravimetric feeders' hoppers under a small flow of dry nitrogen. In the case of the NFC masterbatch, which consisted in a grinded foam (obtained by freeze drying), the lower rate of feeding was limited to 0.1 kg/h in NFC.

- Screw configuration, speed and temperature profile:

Different screw geometries were tested to optimize material mixing and residence time. Variations in screw speed were also evaluated to balance throughput with proper blending. Trials demonstrated that a high screw speed not only ensured to feed all materials up to 10 kg/h, thus avoiding material build-up or inconsistent feeding, but also improved degassing efficiency facilitating better removal of moisture or volatiles during processing. At a speed of 700 rpm, a vacuum of 500 mbar could be obtained, which could still be optimized.

There was no specific challenge in adapting the temperature along the screw profile. The melting zone were set at 200 °C, which is well above the melting point of PLA, but unnecessary high in the case of PLA Luminy LX175 based compounds. The rest of the profile was set at 190 °C and the die was maintained at 185 °C to ensure a good strength for the strand allowing quick cooling in an 18 °C water batch followed by pelletizing. Temperatures and screw speed were set in order to fix the torque below 70 % of the max torque, to avoid that any mistake in feeding would torque the engine out, thus stopping the process.

- Grinder performance:

Slight adjustments were made to the grinder setup (knife-speed and strand pull speed) when working at 10 kg/h. Producing two strands thanks to a two-holes-die helped divide the cutting speed by two, thus avoiding reaching the maximum speed of this side equipment. Pellets meeting the PL15 specifications (in terms of circularity and length) were obtained with a rather high amount of humidity, thus requiring further drying before further processing in PL15.

Table 3: Main compounding parameters

Output (kg/h)	10
Temperature (°C)	200 / 190 / 185
Melt temperature at the die (°C)	210
Degassing pressure (mbar)	500
Screw speed (rpm)	700
Engine torque (% of max torque)	65
Melt pressure at the die (bar)	35

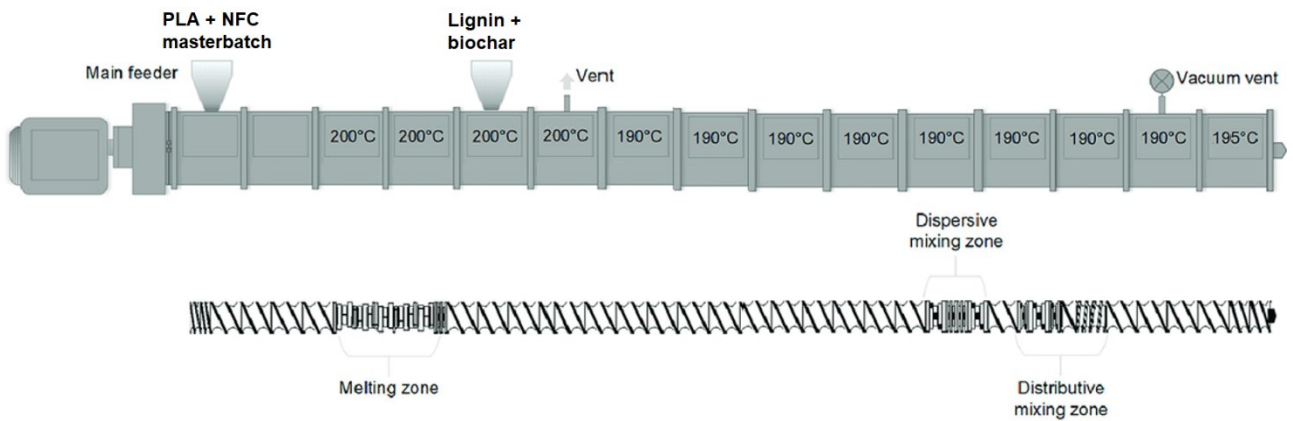


Figure 11: Screw profile, temperatures and introduction points



*Figure 12: Obtained granules*

## 4.5 PL15 -AIMEN

### 4.5.1 Printability tests on commercial PLAs

PLA was approved and accorded to be used as polymeric matrix to develop bio-compounding to be validated in TeC4. The final printable nanocomposite will contain BIOMAC fillers: biochar, nanolignin and nanocellulose. Studies on thermal and physical properties of different commercial PLA were carried out to select the optimum considering the extrusion and printing processes: DSC, TGA and rheology. The three different commercial PLA considered were: PLA Ingeo, PLA Luminy and 20% NC reinforced PLA) and PLA, UPM Formi 3D loaded with nanocellulose fiber, which is as well a material produced within BIOMAC ecosystem. Figure 13 shows results corresponding to DSC, TGA and rheology tests for the three of them.

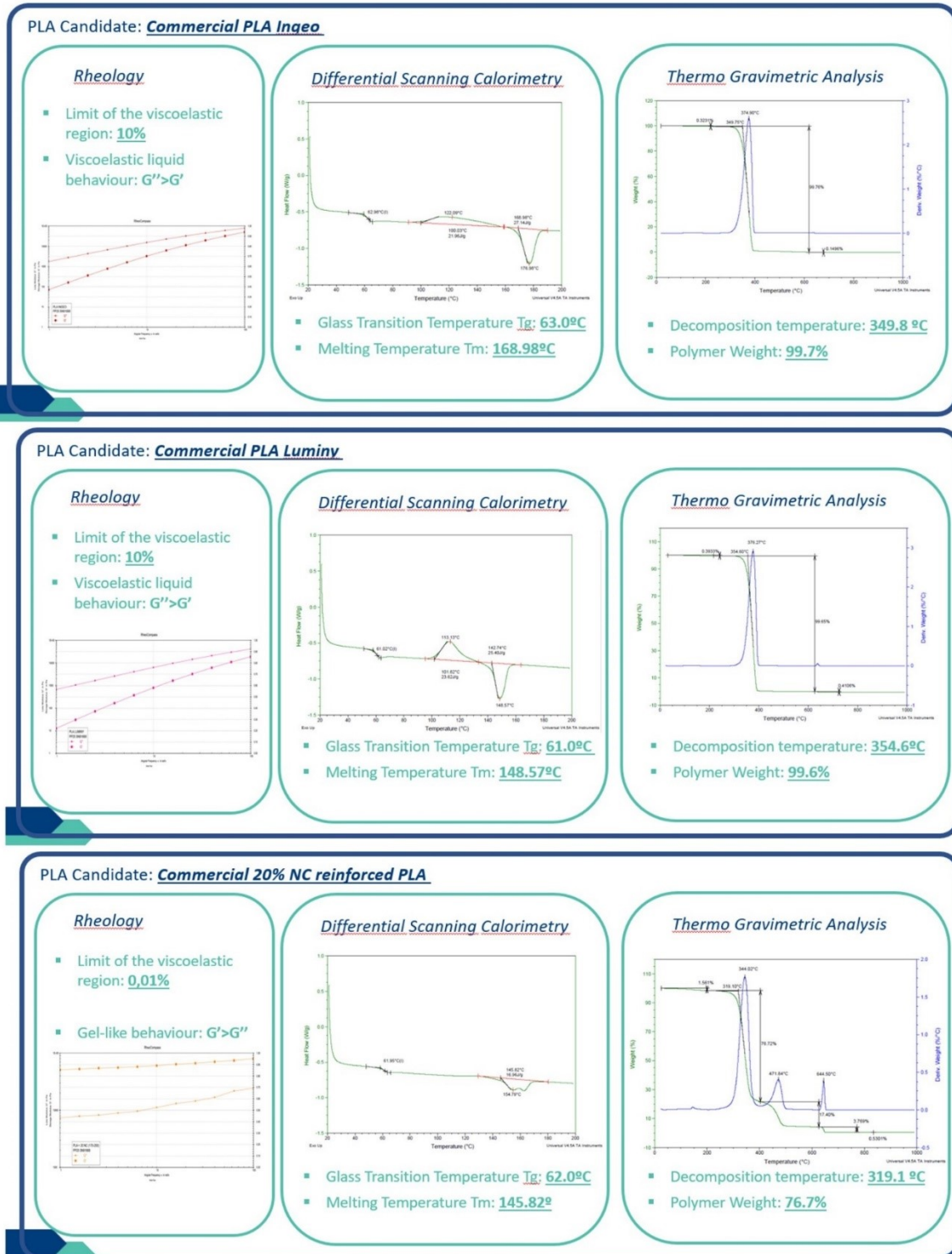
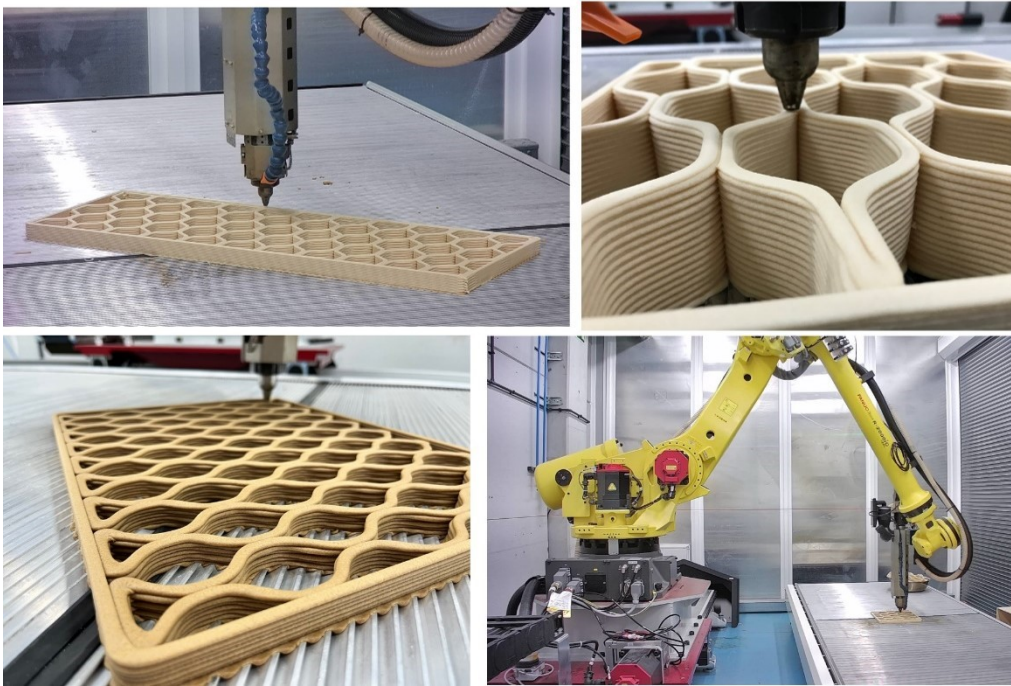


Figure 13: Results corresponding to DSC, TGA and rheology tests for the three different commercial PLAs.

On the one hand, PLA reinforced with 20% NC presents a lower temperature of degradation. The 20% NC load presented in this material might bring some inconvenient considering the three different fillers to be used in the final composite. Also, according to rheology measurements, viscoelastic limit is very low. Nevertheless, is a good candidate in terms of printability. On the other hand, even if Ingeo and Luminity

present similar rheology behaviour and temperature of degradation,  $T_m$  of Luminity (150°C) is lower than that corresponding to Ingeo (170°C). To make Ingeo printable at 160°C the use of plasticizers might be necessary.

Considering this, Luminity was the recommended to be selected to manufacture the final TeCa4. Large format printability tests of the honeycomb structure by ACCIONA were as well carried out using Luminity with successful results (Figure 14).



*Figure 14: Printing test to evaluate large format printing process on commercial PLA.*

Additionally, during printing process, a thermal camera was used to monitor the thermal distribution over the part while manufacturing (thus avoiding warping and shrinkage effects on the final parts based on thermal measurements, as well as good adhesion between layers of the parts) (Figure 15). CAD design provided by ACCIONA was used. Some of the parameters that were being into consideration were: printing orientation (to maximize mechanical performance on the main load direction for in-service conditions), extrusion and printing speed, nozzles / printing bed / environmental temperatures are being evaluated to minimize the residual stress, shrinkage, and warpage within the manufactured bridge module. These manufacturing speeds and temperatures were measured in real-time and will serve as process feedback to optimize the interlayer adhesion factor, which is limiting for this technology. As this has the greatest impact on the mechanical performance of the parts, it will be possible to keep the interlayer material temperature close to the melting temperature and significantly improve both the quality and properties of the part.

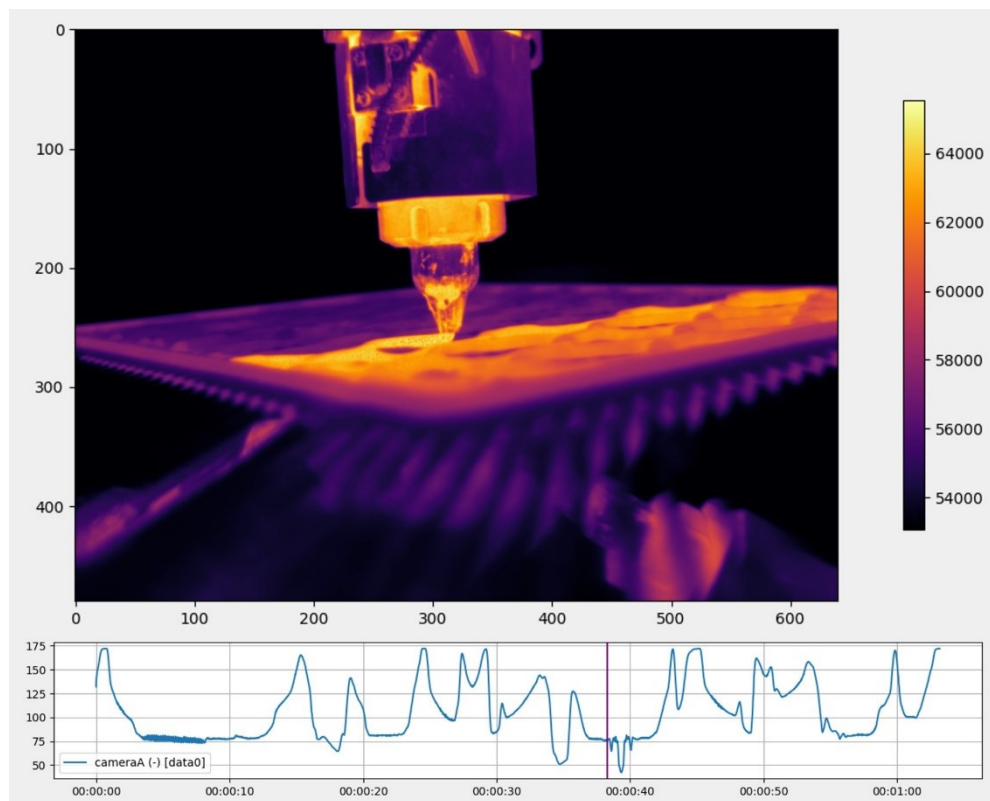


*Figure 15: Monitoring systems are being applied to ensure the quality of large-size printed parts.*

#### 4.5.2 Printability tests on BIOMAC based PLA bio-compounding

Printability tests on final BIOMAC compounding for TeC4 took place. The following parameters and actions were selected to optimize the printing process:

Table 4: Main printing parameters

Nozzle (mm)	4
Temperature (°C)	160 / 170 / 180 / 170
Layer height (mm)	1.5
Shape (mm)	310 x 310
Height (mm)	330
Print speed (mm·s <sup>-1</sup> )	27
Layer time (s)	46
Bead width	8,45

- Reduced drying time to 3 hours at 50°C and stirred before printing to prevent agglutination.
- Degradation likely at 60°C, printing at 175°C solved the issue.
- Slow printability to avoid extruder motor reaches torque limit (see Figure 16).

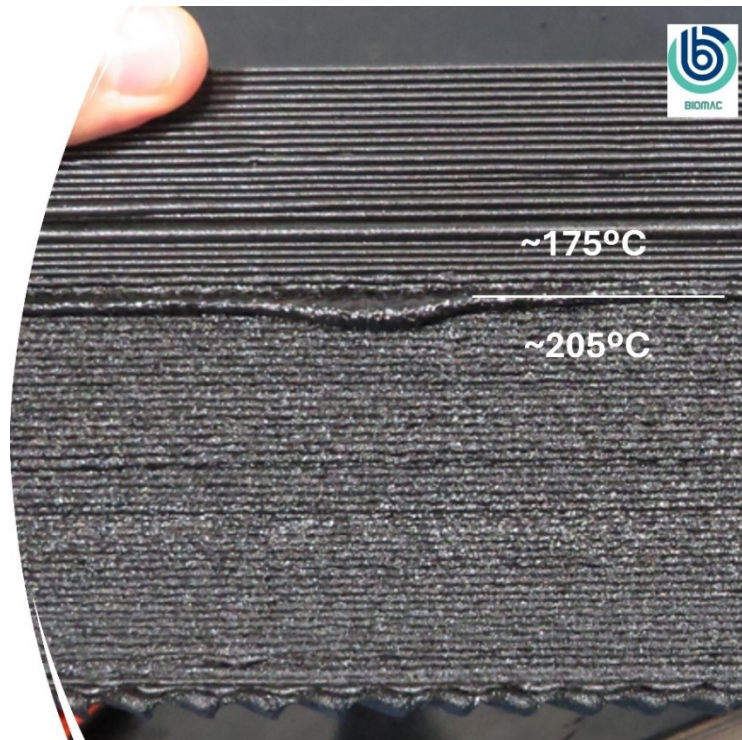


Figure 16: Agglutination during printing process

- Maximum 10-12 RPM and 25mm/s for 1.5mm layer height and 8mm bead width.
- Added external IR lamps to control cooling speed and increase base layer temperature for better layer adhesion.

As a result, good surface quality and zero warping panels were manufactured to produce both flexural and tensile coupons to be analyzed by ACCIONA. The overall print is successful, and a full side cubic perimeter is obtained (see picture below).



*Figure 17: Printed cubes in PL15 using LIST compounding based in PLA*

Also, printability tests on final BIOMAC geometry for TeC4 have been already carried out: Honeycomb structure to be integrated in a core-shell design by ACCIONA. During this procedure, IR was used at two sides and a small overheating at the middle of the print, so the process is stopped, the IR set further and print restart. As a result, one side loses the perfect shape, and one of the edges with material accumulation. The print is successful, and the samples were sent to ACCIONA (see Figure 17). The following parameters and actions were selected to optimize the printing process:

*Table 5: Main printing parameters*

Nozzle (mm)	4
Temperature (°C)	160 / 170 / 180 / 170
Layer height (mm)	1.5
Shape (mm)	310 x 310
Height (mm)	60
Print speed (mm-s-1)	27
Layer time (min)	7
Bead width	8,45

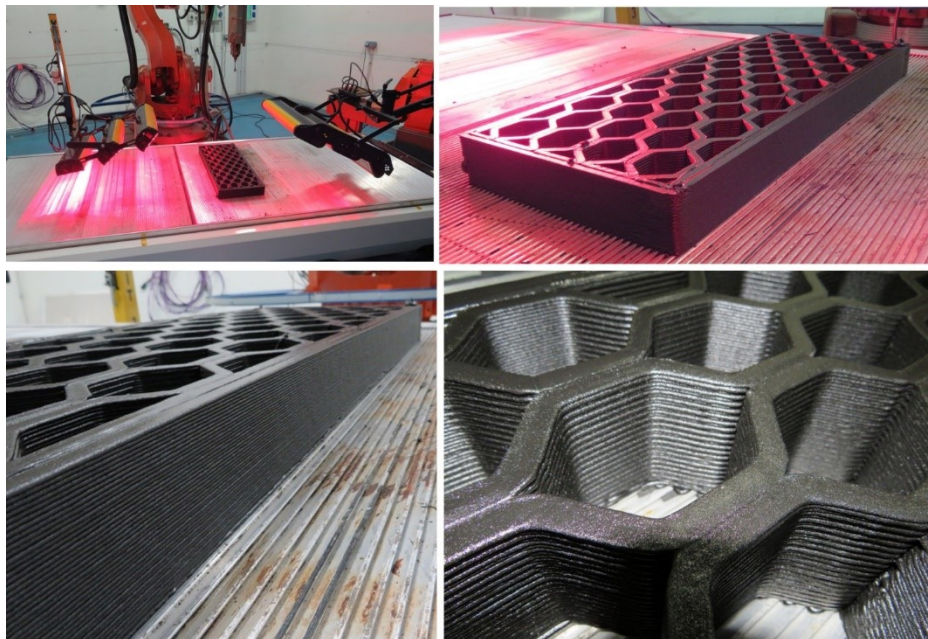


*Figure 18: Honey comb structure printed in PL15*

#### 4.5.3 Demo manufacturing

Once the suitability of final compounding for structural applications was confirmed, containing 79.21 % PLA Luminy, 9.9 % Biochar, 9.9% lignin, and 1% nanocellulose, the next steps focused on designing and printing a mocap module of a pedestrian bridge. As shown in the Figure 19, the design concept revolves around a honeycomb core structure, chosen to replicate the manufacturing conditions and dimensions

of a verified piece while optimizing mechanical performance. The primary objective is to evaluate the composite's suitability for structural applications, in addition to showcasing the potential and versatility of additive manufacturing (AM).

The honeycomb core was sandwiched between two glass fiber skins, creating a composite panel measuring 2000 × 600 × 75 mm. To facilitate integration, holes along the perimeter will allow for the embedding of structural rails.

Two distinct rail designs are proposed:

1. Rail 1 – Printed vertically with a double-wall structure, enhancing mechanical resistance in the primary load direction.
2. Rail 2 – A modular system based on flat panels and column supports, mirroring the honeycomb base printing strategy for easy assembly.

To further explore AM capabilities, design diversity was prioritized, incorporating geometric variations that optimize structural behavior and material efficiency.

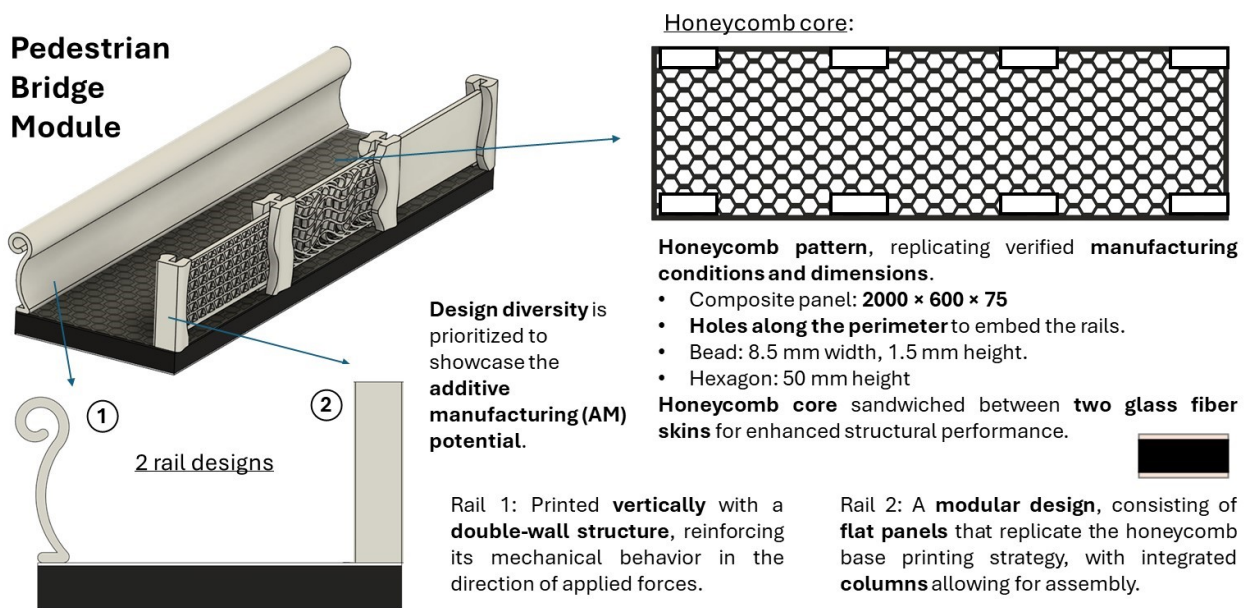


Figure 19: Resume of initial desing for pedestrian bridge module

The printing process consisted of three interconnected stages, each playing a crucial role in the final outcome:

1. CAD Modeling: The process begins with the creation of raw CAD models, which primarily define the basic geometry of the components. These initial models are compact structures with well-defined edges, focusing on shape rather than printability.

2. Path Planning: The CAD models are then imported into AdaOne, the path-planning software, where they are optimized for printing. At this stage, bulk structures are modified to accommodate manufacturing constraints. The standard printing parameters include:
  - Nozzle diameter of 4 mm
  - Layer height: 1.5 mm
  - Single-wall extrusion (8.5 mm width)
  - Bed temperature: 60 °C
  - Continuous printing mode (eliminating travel moves)
  - 20% overlap between the skin and the infill (when is required)
  - First layer start from automatic (specific parameters. Printing speed: 10 mm/s, Extrusion: 10 RPM)
  - External heating with IR lamps
3. Printing Execution: Once the toolpath is finalized, the trajectory is uploaded to the robotic controller, where processing conditions are fine-tuned to match system requirements. Adjustments such as the spacing between walls, infill density, and printing speed are made to optimize print quality for different components.

This structured approach ensures that the transition from digital model to physical print is smooth, efficient, and adaptable to varying design requirements.

#### Step 1: Panels printing (Rail type 2)

The Rail Type 2 was selected as the first component to be printed due to its role in the optimization process, providing crucial data for scaling up to larger and more complex pieces. The primary objective of these prints is to refine the printing strategy, particularly in accommodating the holes incorporated into the honeycomb core—a feature absent in the original test models but highly influential in path planning.

A key challenge arises from hardware limitation. The extrusion process cannot be stopped mid-print without causing catastrophic errors, compromising both the structural integrity and aesthetic quality of the component.

As shown in Figure 20, Rail Type 2 consists of seven distinct pieces, each tailored to its position within the bridge structure. These pieces vary in patterns and geometries, demonstrating additive manufacturing's adaptability to diverse design requirements. The components are categorized into columns and panels. Columns are embedded within the honeycomb core and feature an H-shaped geometry to support the panels. Among the four columns, two are positioned at the bridge edges, designed with a single slot for panel attachment, while the two central columns feature dual slots, allowing them to connect multiple panels.

This modular approach highlights AM's flexibility, enabling rapid design adaptation while ensuring structural feasibility.

The optimization of the panels was carried out in three stages to ensure proper adaptation to the final base requirements:

4. **Honeycomb Pattern Optimization:** The process began by refining the honeycomb pattern to match the processing conditions of the final structure. This was achieved by printing small-scale test panels (250 × 250 mm) and adjusting parameters accordingly.
5. **Scaling to Full Panels:** Once the optimal settings were established, they were applied to Panel 1 and Panel 2, ensuring consistency across different components.
6. **Panel 3 Design Adaptation:** Unlike the first two panels, Panel 3 was designed using AdaOne's built-in path-planning infill options, which allowed for a rapid adaptation of patterns without requiring additional manual adjustments.

The processing parameters for all panels are summarized in Table 6. Across all cases:

- Infill density: 35%
- Total initial height: 35 mm
- Final height after machining: 25 mm (to fit the assembly requirements)

In all the cases the prints were 100% successful, because of the previous optimization process. As expected from previous test printing, the layer time was large enough to induce complete layer cooling. Consequently, the substrate temperature during extrusion was defined by bed temperature and kept around 60°C. However, the melting temperature of composite and the extruded volume of material ensures the correct layer adhesion.

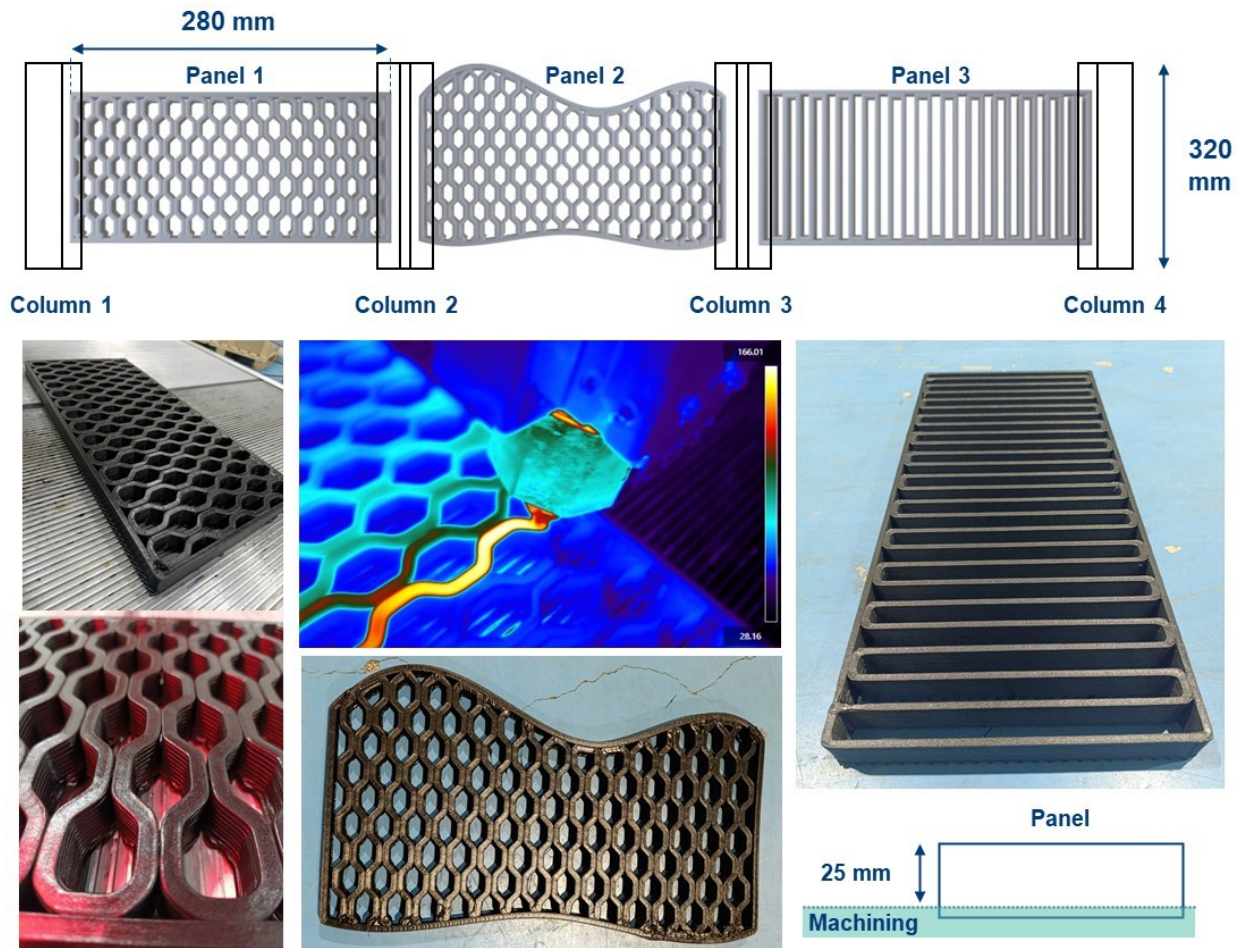


*Figure 20: Overview of Rail Type 2 (top): A modular system consisting of four columns designed to be embedded into the honeycomb base, along with three connecting panels, each featuring distinct geometries. Bottom section: Images of the three different printed panels: Honeycomb square panel (left), Honeycomb wavy panel (middle), Straight panel (right). Bottom right corner: Schematic detailing the machining process required to refine the raw printed pieces into their final components.*

As part of the exploration of more complex pattern designs, the triangular infill was tested to take advantage of the built-in path-planning software options while maintaining a continuous printing strategy (Figure 21). However, despite its feasibility, this pattern required multiple layers with varying orientations, leading to material accumulation at layer intersection points. This buildup resulted in intolerable defects, compromising both print quality and structural integrity. Consequently, despite being printable, the triangular infill was discarded due to its incompatibility with the required manufacturing standards.

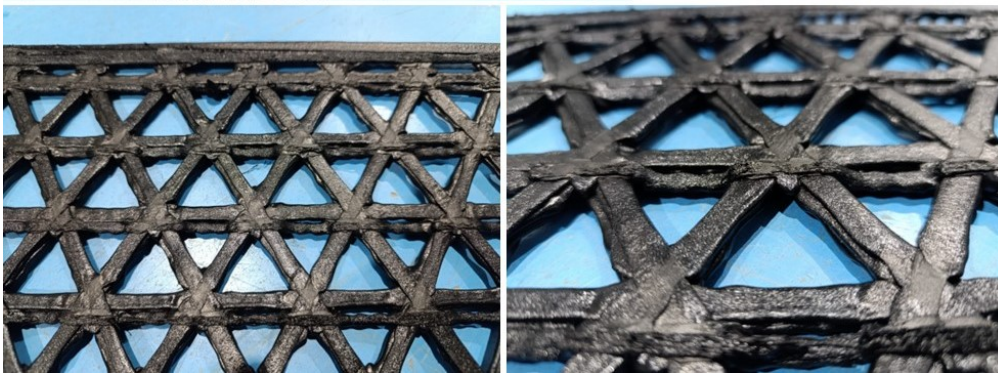


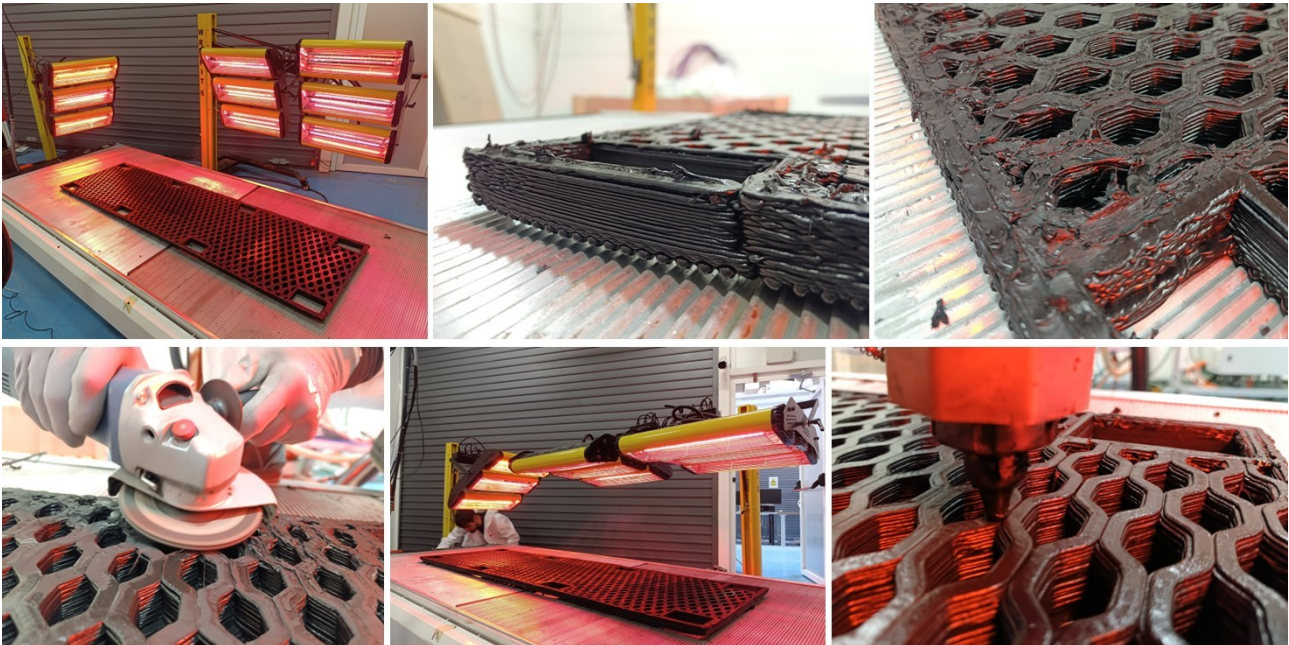
Figure 21: Non successful panel geometries.

Table 6: Processing conditions for different components

		Panels Rail type 2	Honeycomb core	Columns Rail type 2	Rail type 1
Infill	%	34	34	0	0
Extruder T1	°C	165	160	160	160
Extruder T2	°C	170	170	170	170
Extruder T3	°C	190	195	200	200
Nozzle	°C	190	190	200	200
Printing speed	mm/s	27	25	36	18
Extrusion speed	RPM	11	13	11	8

### Step 2: Honeycomb core printing

For honeycomb core printing, the processing parameters for honeycomb panels were extrapolated. As shown in Figure 22, to minimize heat loss from the substrate, the entire print bed (1.5 x 3 m) was surrounded by infrared (IR) lamps. Given the large dimensions of the printing room (approximately 5 x 5 x 4 m), heating the entire volume is not feasible. The IR lamps provided radiative heating directly to the surface of the printed object, allowing for efficient surface heating while minimizing the energy required to reach high printing temperatures. This approach improved layer adhesion and reduced internal stresses caused by the cooling and contraction of the thermoplastic material.



*Figure 22: Images of the honeycomb core printing process. Top row, from left to right: Overview of the honeycomb core structure setup, including external IR lamps, detail of structure warping, and warping-induced defects. Bottom row, from left to right: Detail of the defect sanding process, IR lamp setup for surface heating before printing restart, and close-up of the bead during printing.*

The printing process remained stable for over 15 hours of continuous operation, demonstrating the composite's suitability for large-scale printing and its negligible impact on extruder torque limits. However, due to the large size of the demonstration piece, significant material contraction occurred. The high material volume required for the print made it impossible to predict these contractions in advance. Consequently, both the edges and the central area—where bed adhesion was compromised due to a gap in the print bed—experienced warping. This deformation caused a slight increase in the height of the top layer, leading to nozzle clogging and surface defects, ultimately making it impossible to continue printing.

To recover a smooth printing surface and restart the process, the entire surface was sanded using rotary power tools. Additionally, IR lamps were positioned 30 cm above the surface to heat the structure and restore the processing conditions prior to the stop. This approach allowed for a successful printing restart, enabling the completion of the initially designed demonstration piece. To compensate for the thinner regions caused by material contraction, an additional 15 mm (equivalent to 10 layers) was added on top of the planned printing path.

### Step 3: Rail type 2 columns printing

To complete the printing of rail type 2, the columns were printed. The original printing strategy aimed to print the columns one by one, in a vertical orientation, to analyze the composite behavior under new processing conditions. However, as shown in Figure 23a, this strategy resulted in short layer times, which, due to the composite's cooling dynamics, were insufficient to ensure proper solidification of the bottom layers. Consequently, the columns collapsed, leading to unacceptable results.

To address the cooling dynamics while working with the minimum flow rate allowed by the hardware, a second attempt was made by increasing the layer height to 3 mm. This new configuration allowed for good-quality parts, but it was not compatible with the available resources and time constraints.

In a third attempt, multiple columns were printed simultaneously to increase the layer time while maintaining the original printing conditions (1.5 mm layer height and 8.5 mm bead thickness). However, as shown in Figure 23b and 28c, this strategy caused excessive layer cooling, which reduced interlayer adhesion and significantly affected the mechanical performance of the printed components. As a result, the printed parts cracked and had to be discarded.

The final strategy combined the previous approaches by printing two columns at a time. This method reduced the layer time and improved layer adhesion. As shown in Figure 23d, this approach resulted in high-quality, defect-free samples with homogeneous layer deposition. To prepare the successful prints for the final demonstrator assembly, the printed samples required machining as illustrated in Figure 23d (right).

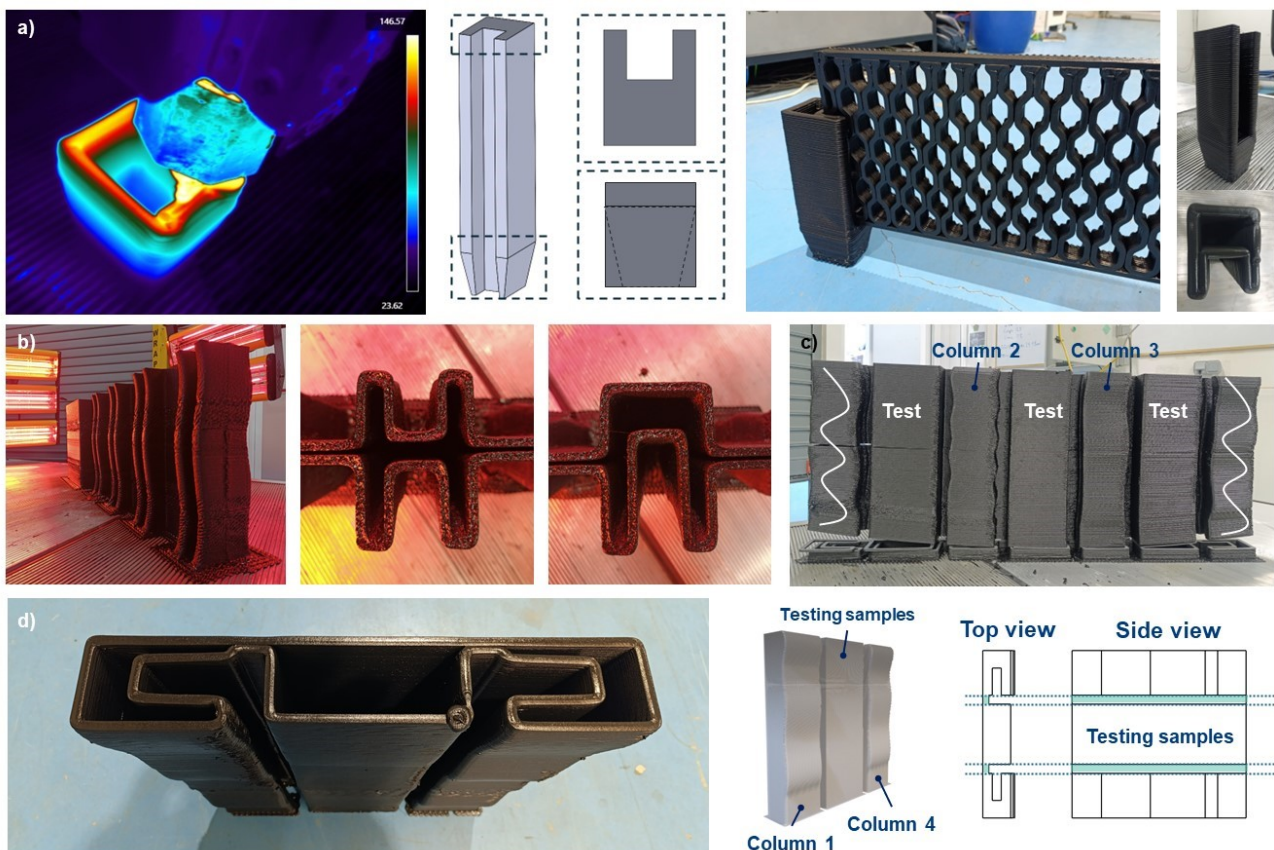


*Figure 23: Summary of representative images for column manufacturing. a) From left to right: Infrared thermal camera images during single-column printing, graphical representation of side columns (including top and bottom views), assembly of a single column and panel, and details of the printed single column. b) From left to right: Image of the first printed column array, including details of side and middle columns. c) Image of the second printed column array, showing defects caused by poor layer adhesion. d) From left to right: Image of the third column array and plans for its post-processing.*

#### Step 4: Rail type 1 columns printing

Finally, the printing of rail type 1 was addressed. To test new printing conditions and explore the manufacturing potential, rail type 1 was designed to be printed horizontally as a single-wall structure with a hollow core. This strategy allowed the component to work in the most stable direction (the x-axis), enhancing mechanical stability and improving the durability of the components.

The initial idea was to print the entire rail in one piece. However, due to hardware limitations and assembly requirements, the rail was divided into three sections. Each section includes two protrusions at the bottom and the top that allow pieces fitting into the honeycomb core's embedded holes.

Figure 24 shows the printing process of rail type 1 and optical images of the final components. The printing strategy and layer time resulted in stable, defect-free, high-quality prints. The design considered the limitations of additive manufacturing, and to avoid overhangs, the top protrusion was angled. Despite the challenges this strategy presented, the print was successful.

To prepare the final pieces, the angled sections had to be machined, along with the top and bottom surfaces of the components, to match the dimensions of the honeycomb core.



Figure 24: Images of rail type 1 and its printing process.

#### 4.6 Final demonstrator – ACCIONA

At the beginning of the project, Acciona evaluated the different commercial polymers available on the market to establish realistic mechanical properties to aim for in the project. The following products were analyzed: TPU HARDNESS+, TPU Flexfill 98A, and commercial TPU reinforced with chopped CF. Below is a table with the obtained mechanical results.

Material	Hardness+	CF Reinforced	Flexfill 98A
$\sigma_{xy}$ (MPa) (2%)	29,6	18,4	2,2
$\epsilon_{xy}$	2%	2%	2%
$E_{xy}$ (GPa)	1,52	0,92	0,11

Table 7: Main compounding parameters

It was ultimately concluded that a  $\sigma$  value of 25 MPa in the principal direction represented the upper limit achievable by the consortium. Consequently, the footbridge had to be designed with this constraint in mind.

Several numerical models were developed, leading to the determination that thermoplastics, due to their low mechanical properties and significant creep effects, are not suitable for permanent structural applications. The solution was to design a composite structure, utilizing the material developed in the project as the core of a sandwich panel, with fiberglass skins on the top and bottom surfaces

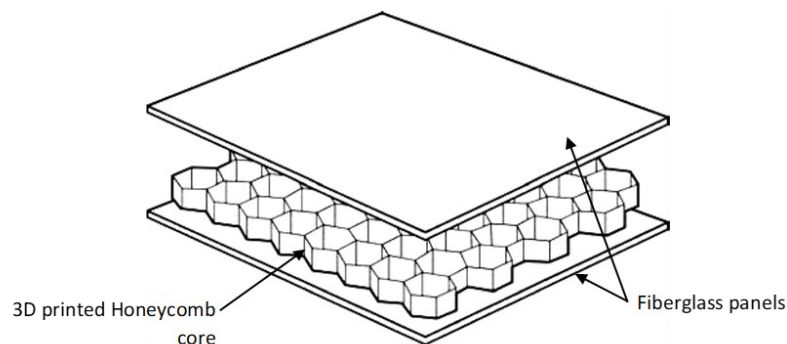
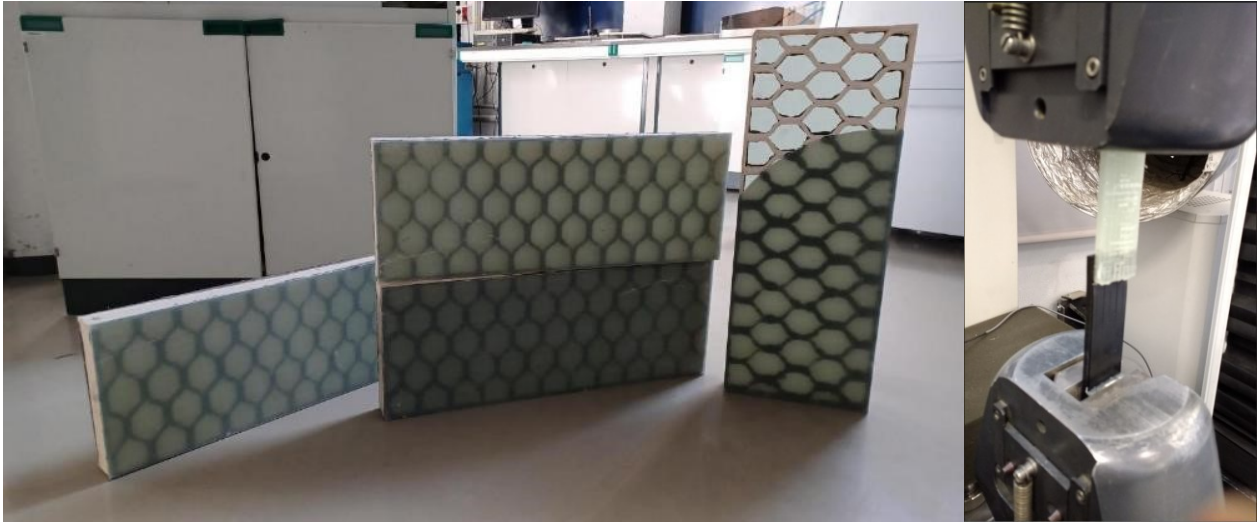


Figure 25: Example of a structure with a sandwich panel shape

These types of structures offer high strength with minimal weight. Additionally, 3D printing enables precise shaping of the core, optimizing its geometry to enhance mechanical performance and minimize material waste. This technology allows for the design of customized structures with specific configurations that maximize efficiency and adaptability for various applications.

In such structures, the core primarily withstands compression and shear forces. For this reason, Acciona collaborated with Aimen to develop tests that could simulate the mechanical behavior of the material under real load conditions. These tests were designed to assess the shear and compression resistance of the honeycomb panels.



*Figure 26: Sandwich panels created for short beam tests on the left, and lap shear test to evaluate the adhesive on the right.*



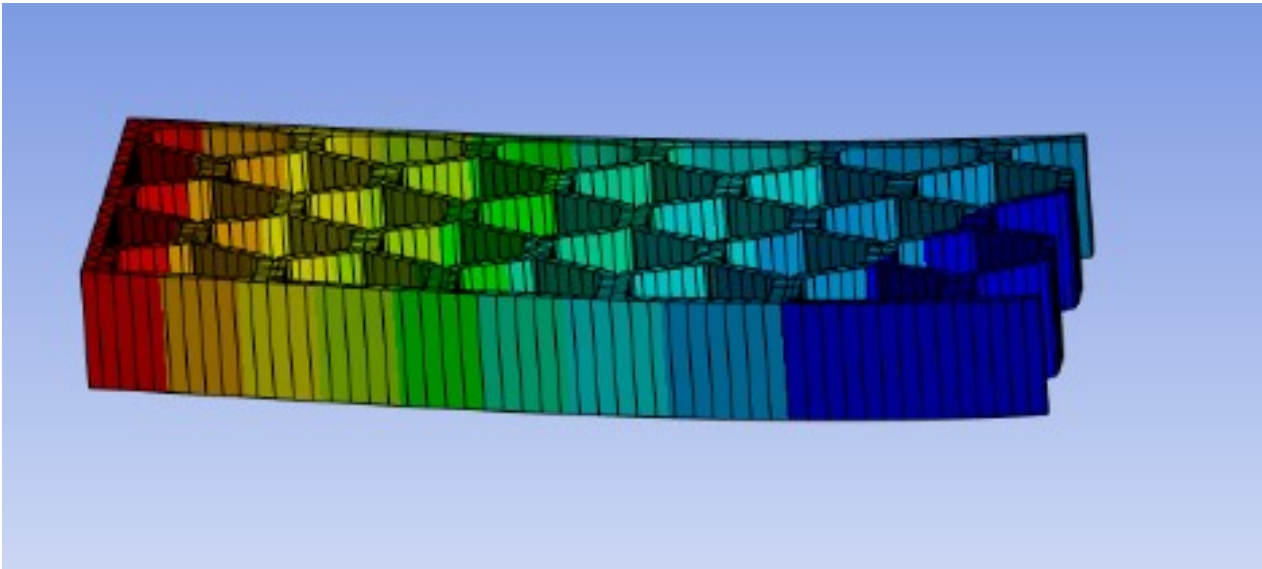


Figure 27: Short beam test above and numerical model below.

Once the necessary mechanical properties were determined, the first numerical simulations of the final footbridge could be conducted.

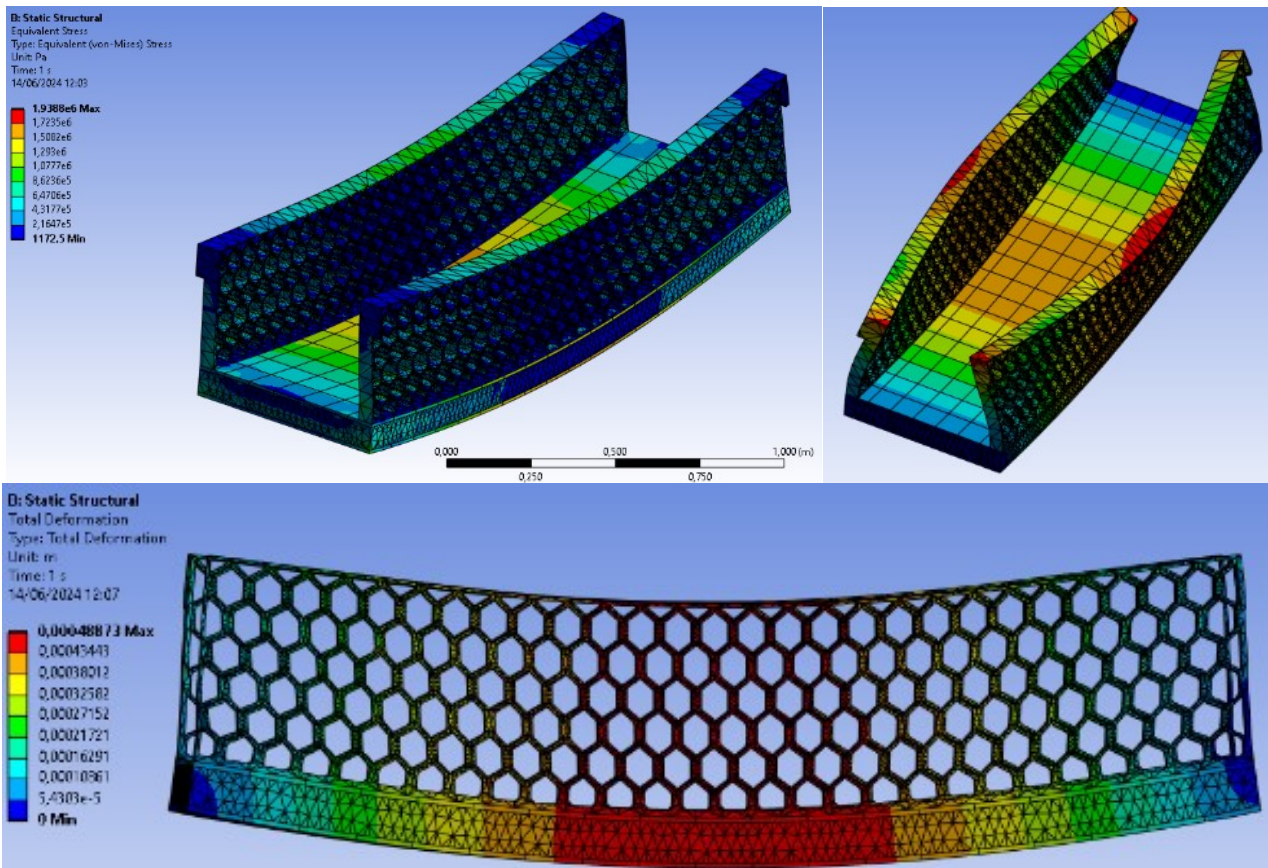
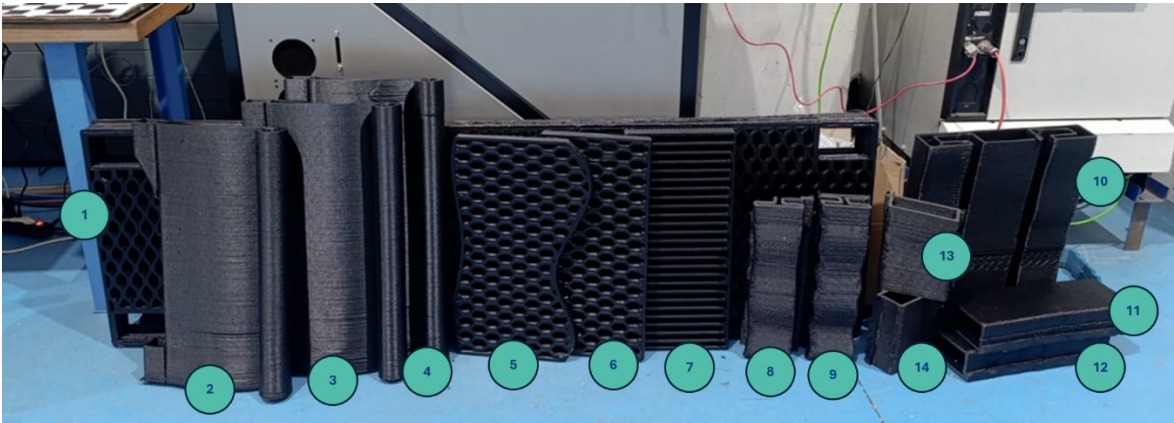


Figure 28: Short beam test above and numerical model below.

#### 4. Demonstrator assembly

Acciona received the modules from PL15 in February 2025.



1	Slab	4	Handrail 3	7	Panel 3	10	Column 3, 4, panel
2	Handrail 1	5	Panel 2	8	Column 1		
3	Handrail 2	6	Panel 1	9	Column 2	11 -14	Other

*Figure 29: All the modules printed by AIMEN and sent to Acciona for the assembling process.*

In addition to the parts provided by AIMEN, the assembly required the fabrication of fiberglass skins through infusion to provide the deck with its structural capacity. For this purpose, 5 mm thick skins were designed using five layers of fiberglass fabric of 800g/m<sup>2</sup> weight, infused with epoxy resin using the vacuum technique. After curing at 80°C for 8 hours, the slabs were cut to the required dimensions.

The 3D-printed parts had to be cut, sanded, and adjusted to ensure proper assembly while also addressing printing defects to allow the modules to fit together. AIMEN prepared the necessary cutting plans; however, as the assembly progressed, additional modifications were required to complete the footbridge. The modifications included:

- Lowering the deck module due to its curvature. This defect was identified during manufacturing, so the module was printed with extra thickness to allow for correction by milling, ensuring the final physical properties of the slab were not compromised.

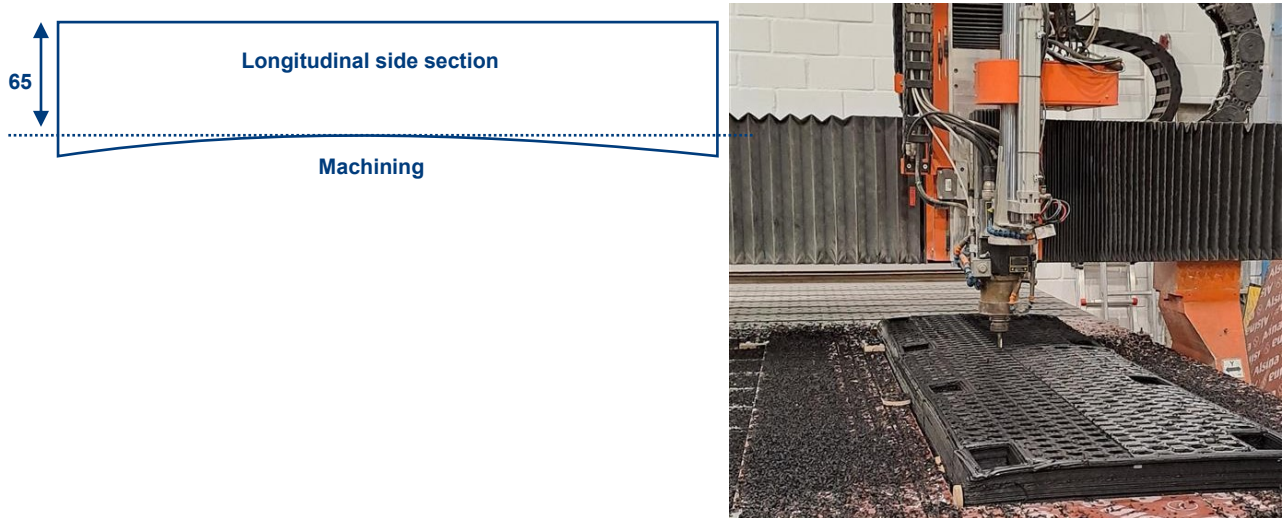


Figure 30: Modification in printed basement (left: planning; right: CNC milling)

- Grinding the length of the handrails:

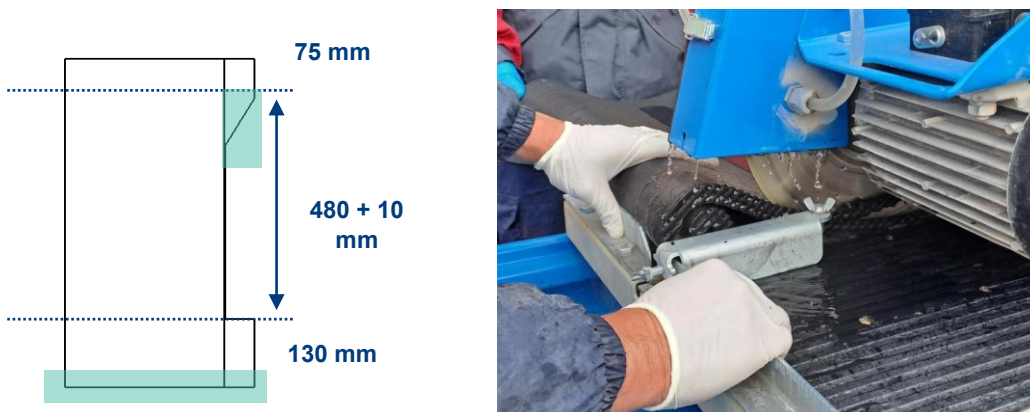


Figure 31: Water-cooled cutting of the module

- Trimming the columns

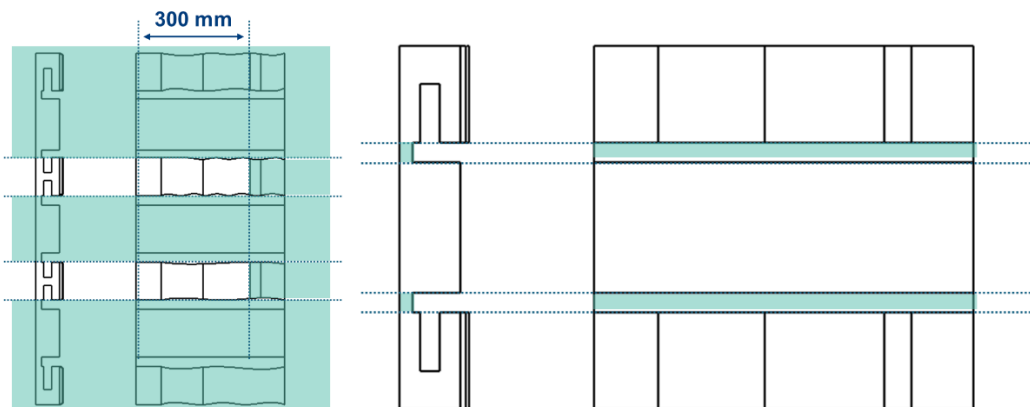


Figure 32: Planning of the column extraction

- Rectifying the height of the panels and creating sockets so that they slide along the support columns:

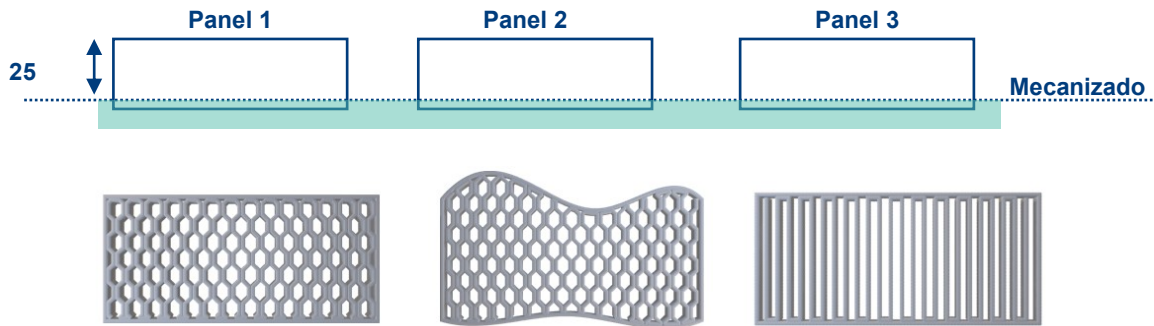


Figure 33: Planning of the panel rectification

After the part grinding process, the assembly began. First, the fiberglass laminates were bonded to the base using the structural adhesive tested in the previous stages. The surface layer was then painted to improve the appearance of the slab (Figure 35). Next, the columns and railings were assembled, and once positioned in their designated locations, epoxy resin was applied to secure and adhere them to the base (Figure 35)



Figure 34: Basement assembling



Figure 35: Assembling of all the modules on the left. Railings and columns fixed with epoxy resin on the right.

The footbridge, once assembled, is shown in Figure 36.



Figure 36: Final demonstrator

## 5 Conclusions

The activities carried out within the framework of TeC4 have advanced the understanding of biobased polymer's behavior and their feasibility for large-scale 3D printing. PLA was selected, a biopolymer that has proven to be compatible with large-format manufacturing while offering better mechanical properties and thermal stability for the construction sector. Additionally, the possibility of combining PLA with (nano)renewable fillers developed within the consortium suggests that adequate reinforcement levels can be achieved for its application in TeC4.

The fabrication of the demonstrator required several modifications to the printed components to ensure proper assembly and fit, including adjustments to module heights, precision machining, and the use of structural adhesives for component fixation. However, overall, the results obtained have demonstrated the feasibility of using PLA reinforced with biobased fillers for the 3D printing of construction structures.